

# Constraining photohadronic scenarios for the unified origin of IceCube neutrinos and ultrahigh-energy cosmic rays

Shigeru Yoshida\*

*Department of Physics, Graduate School of Science, Chiba University, Chiba 263-8522, Japan*

Kohta Murase†

*Department of Physics; Department of Astronomy & Astrophysics; Center for Multimessenger Astrophysics,  
Institute for Gravitation and the Cosmos,  
The Pennsylvania State University,  
University Park, PA 16802, USA*

*and*

*Center for Gravitational Physics,  
Yukawa Institute for Theoretical Physics,  
Kyoto University, Kyoto, Kyoto 606-8502, Japan*

(Dated: September 11, 2020)

The diffuse neutrino flux measured in IceCube is comparable with the ultrahigh-energy cosmic ray (UHECR) flux, which has led to the concept of a unified origin of high-energy neutrino and UHECR backgrounds. We construct a generic unification model of sources to explain UHECR data at  $\gtrsim 10^{19}$  eV, and high-energy neutrinos with energies that exceed  $\sim 100$  TeV in the framework of photo-meson production processes, and provide general constraints on the source properties. A source environment with moderately efficient in-situ production of  $\gtrsim 100$  TeV neutrinos with an optical depth of  $0.1 \lesssim \tau_{p\gamma} \lesssim 0.6$  must be realized to accelerate cosmic rays to ultrahigh energies. The measured fluxes of cosmic rays and neutrinos set a bound on the source luminosity and its rate density. Although the results are rather general and applicable to unknown source population, among the proposed source candidates, low-luminosity gamma-ray bursts (GRBs) and tidal disruption events (TDEs) could satisfy the requirements if the Lorentz bulk factor of plasma outflow and the equipartition parameters for cosmic rays and magnetic field are appropriately selected.

PACS numbers: 98.70.Sa, 95.85.Ry

## I. INTRODUCTION

The detection of cosmic neutrinos in the energy range from  $\sim 10$  TeV to  $\sim$  PeV by the IceCube Neutrino Observatory [1–4] raises interesting questions. The observed energy flux of high-energy neutrinos seems to be comparable to that of ultrahigh-energy cosmic rays (UHECRs) at  $\gtrsim 10^{19}$  eV. Is the origin of high-energy neutrinos related to the UHECR sources? Is the comparability of neutrino and UHECR fluxes a consequence of yet-unknown common astrophysical phenomena? Several studies have been reported in the literature to probe these questions, mainly in the framework of hadronuclear ( $pp$ ) collisions inside cosmic-ray reservoirs [5] – jetted active galactic nuclei (AGN) embedded in clusters and groups of galaxies [6], starburst galaxies [7, 8], or phenomenological setups used for UHECR observations [9]. Remarkably, these cosmic-ray reservoir models can even explain the diffuse isotropic gamma-ray background in the sub-TeV range, measured by the *Fermi* satellite [6, 8]. High-energy neutrinos can be produced, including by photohadronic interactions ( $p\gamma$ ) inside cosmic-ray emitters (e.g., Ref. [10]). The photo-meson production process may occur simultaneously or in succession to the

acceleration of cosmic rays. If the power of cosmic-ray particle emitters is sufficiently large, it is indeed possible to emit both  $\gtrsim 100$  TeV neutrinos and UHECRs. Various astrophysical models have been investigated, which include classical high-luminosity (HL) gamma-ray bursts (GRBs) [11, 12], low-luminosity (LL) gamma-ray bursts [13–15], new-born magnetars [16–18], tidal disruption events (TDEs) [19–21], and blazars [22–26].

In this report, we examine a generic unification model to account for observed neutrinos with energies greater than 100 TeV and UHECRs in the photo-meson production scheme. The cumulative neutrino background flux is estimated analytically using parameters to characterize sources such as the photon luminosity and the source number density. The UHECR flux is also estimated semi-analytically by considering their collisions with background photons in intergalactic space. We also derive the source requirements for the acceleration of cosmic-ray protons to ultrahigh energies, and transform them into the criteria of the parameters relevant to high energy neutrino emissions such as the optical depth of  $p\gamma$  interactions. The estimated fluxes of neutrinos and UHECRs from sources that satisfy these criteria are compared to the measured flux at  $100 \text{ TeV} \lesssim E_\nu \lesssim 10 \text{ PeV}$  and its upper limit at  $E_\nu \gtrsim 100 \text{ PeV}$  by IceCube, as well as the measurement of UHECRs at  $10^{19}$  eV. The resultant constraints on the parameters of general source characteristics are presented. We finally describe a case study

\* syoshida@hepburn.s.chiba-u.ac.jp (S. Yoshida)

† murase@psu.edu

for specific astronomical objects such as LL GRBs.

In this work, we use  $E$  for the observed energy,  $\varepsilon = (1+z)E$  is the energy in the engine frame (or the rest frame of the Hubble flow), and  $\varepsilon'$  represents the energy in the comoving frame of the plasma outflow. The standard  $\Lambda$ CDM cosmology with  $H_0 = 73.5 \text{ km s}^{-1} \text{ Mpc}^{-1}$ ,  $\Omega_M = 0.3$ , and  $\Omega_\Lambda = 0.7$  is assumed throughout the report.

## II. CONSTRAINTS DUE TO SOURCE MODELING

### A. UHECR acceleration and survival

In the unification model of UHECRs and IceCube neutrinos, the source to emit  $\gtrsim 100$  TeV neutrinos must also be capable of accelerating cosmic rays to UHEs ( $E_i \gtrsim 10^{20}$  eV) by definition. Some of the required conditions for classification as UHECR emitters are described by relatively simple formulas.

Let us consider a source with an acceleration and emission region that is given by  $R$  measured in the central engine. We also denote the bulk Lorentz factor of this source by  $\Gamma$ . For the source to account for the UHECR acceleration, the cosmic ray acceleration time scale,  $t'_{\text{acc}} = \eta \varepsilon'_i / (ZeB'c)$ , must be faster than the dynamical time scale,  $t'_{\text{dyn}} \approx R/(\Gamma\beta c)$ . In this case,  $\varepsilon'_i$  is the cosmic ray ion energy in the plasma rest frame,  $B'$  is the comoving magnetic field strength,  $Z$  is the atomic number of the cosmic ray ions,  $\beta$  is the characteristic velocity in the source, and  $\eta^{-1} \leq 1$  represents the efficiency of particle acceleration. The condition is transformed to the well-known formula [27, 28],

$$L'_\gamma \geq \frac{1}{2} \xi_B^{-1} c \eta^2 \beta^2 \left( \frac{\varepsilon_i^{\text{max}}}{Ze} \right)^2 \quad (1)$$

$$\simeq 1.7 \times 10^{45} \text{ erg/s } \xi_B^{-1} \eta^2 \beta^2 \left( \frac{\varepsilon_i^{\text{max}}}{Z10^{11} \text{ GeV}} \right)^2,$$

which is equivalent to the Hillas condition in the limit of  $\eta \rightarrow \beta^{-2}$ . In this case,  $\varepsilon_i^{\text{max}} \approx \Gamma \varepsilon_i'^{\text{max}}$  is the maximal energy of UHECRs accelerated at the sources. For a given comoving radiation luminosity  $L'_\gamma$ , the magnetic energy density in the plasma rest frame,  $U'_B$ , is given by

$$U'_B = \xi_B \frac{L'_\gamma}{4\pi R^2 c}$$

$$= \xi_B \frac{L_\gamma}{4\pi \Gamma^2 R^2 c} \quad (2)$$

where  $\xi_B$  is the equipartition parameter. For example, the modeling of GRBs and blazars typically suggests  $\xi_B \sim 10^{-4} - 1$ . As a reference value, the maximum ion energy is set to  $\varepsilon_i^{\text{max}} = 10^{11}$  GeV thorough this work. Indeed, the best fit value for the Auger data is

$10^{10.9}$  GeV [29], so our choice is conservative but reasonable. We also assume the most efficient acceleration case ( $\eta = 1$ ) and a transrelativistic or relativistic source ( $\beta = 1$ ).

UHECRs must be accelerated before cooling via all energy loss processes including synchrotron cooling, i.e.,  $t'_{\text{acc}} < t'_{\text{cool}}$ , where the cooling time (in the plasma rest frame) is  $t'_{\text{cool}} = t'_{\text{syn}} + t'_{p\gamma} + t'_{\text{BH}} + t'_{\text{dyn}}$ , where  $t'_{p\gamma}$  and  $t'_{\text{BH}}$  are the photo-meson production and Bethe-Heitler (BH) energy loss time scales, respectively. The last loss time scale represents adiabatic losses. For a power-law target spectrum, the Bethe-Heitler process is important only if the spectrum is softer than  $\alpha_\gamma \sim 2.2 - 2.3$  [30]. Therefore, we mainly consider cases wherein the BH process is subdominant. The synchrotron cooling time in the plasma rest frame is

$$t'_{\text{syn}} = \frac{4}{3} U'_B \sigma_T c \frac{Z^4}{A^4} \frac{1}{m_p c^2} \left( \frac{\varepsilon_i}{\Gamma m_p c^2} \right) \left( \frac{m_e}{m_p} \right)^2 \quad (3)$$

$$= \frac{4}{3} \frac{\xi_B \sigma_T L'_\gamma}{4\pi R^2} \frac{Z^4}{A^4} \frac{1}{m_p c^2} \left( \frac{\varepsilon_i}{\Gamma m_p c^2} \right) \left( \frac{m_e}{m_p} \right)^2,$$

where  $A$  is the mass number of cosmic ray ions. By requiring  $t'_{\text{acc}} < t'_{\text{syn}}$  at the maximum ion energy in the engine frame ( $\varepsilon_i^{\text{max}}$ ), we obtain

$$B' < \frac{A^4 6\pi e m_p^4 c^4}{Z^3 \sigma_T m_e^2} \frac{\Gamma^2}{(\varepsilon_i^{\text{max}})^2}. \quad (4)$$

In addition, we have another condition to ensure the escape of UHECRs. To ensure that UHECRs can leave the sources before losing their energies via synchrotron cooling, the escape time scale  $t'_{\text{esc}}$  must be faster than  $t'_{\text{syn}}$ . In general, the escape time is model dependent and can be long at lower energies. For conservative estimates, we hereafter assume that the escape time scale is comparable to the dynamical scale in the relativistic environment of the UHECR acceleration site under consideration. This is possible if the escape boundary is comparable to the system size and the magnetic field decays within the dynamical time (see discussion in Ref. [31]). By regarding this ‘‘survival’’ condition as a necessary condition ( $t'_{\text{dyn}} < t'_{\text{syn}}$ ), we obtain:

$$B' < \frac{6\pi A^4 m_p^4 c^{9/2}}{Z^4 \sigma_T m_e^2 (2\xi_B L'_\gamma)^{1/2}} \frac{\Gamma^2}{\varepsilon_i^{\text{max}}}. \quad (5)$$

We utilize Eqs. (1), (4) and (5) as theoretical constraints. We focus on the proton case, i.e.,  $Z = A = 1$ , and discuss the cases of nuclei later.

### B. Photo-meson production

Neutrino emission by the photo-meson production process is characterized by the environment of the target

photons. We start to build our generic framework by defining the reference energy of photons  $\varepsilon_{\gamma 0}$  in the engine frame. Given that a major fraction (but not necessarily all) of photo-meson production in  $p\gamma$  interactions occurs around the  $\Delta$  resonance region (including direct pion production via the  $t$ -channel), we introduce the reference “resonating” energy as

$$\tilde{\varepsilon}_{p0}(s) \approx \frac{(s - m_p^2) \Gamma^2}{4 \varepsilon_{\gamma 0}}, \quad (6)$$

where  $s$  is the Mandelstam variable. In particular, we define  $\tilde{\varepsilon}_{p0}^\Delta \equiv \tilde{\varepsilon}_{p0}(s_\Delta)$ , where  $s_\Delta \approx (1.23 \text{ GeV})^2$  is the square of invariant mass of the  $p\gamma$  collisions at the  $\Delta(1232)$  resonance. Primed (') characters represent quantities measured in the rest frame of plasma with the Lorentz bulk factor  $\Gamma$ . In the present model we approximate the target photon spectrum to be

$$\frac{dn_\gamma}{d\varepsilon'_\gamma} = \frac{K'_\gamma}{\varepsilon'_{\gamma 0}} \left( \frac{\varepsilon'_\gamma}{\varepsilon'_{\gamma 0}} \right)^{-\alpha_\gamma}, \quad (7)$$

where  $\alpha_\gamma$  is the photon index, where we focus on  $\alpha_\gamma \geq 1$ . The normalization photon density  $K'_\gamma$  is bolometrically connected to the source photon luminosity  $L'_\gamma \approx L_\gamma/\Gamma^2$  by

$$L'_\gamma = 4\pi R^2 c \int_{\varepsilon'_\gamma^{\min}}^{\varepsilon'_\gamma^{\max}} \frac{dn_\gamma}{d\varepsilon'_\gamma} \varepsilon'_\gamma d\varepsilon'_\gamma. \quad (8)$$

We have

$$K'_\gamma = \frac{L'_{\gamma 0}}{4\pi R^2 c \varepsilon'_{\gamma 0}} = \begin{cases} \frac{L'_\gamma}{4\pi R^2 c \varepsilon'_{\gamma 0}} \frac{\alpha_\gamma - 2}{x_d^{-\alpha_\gamma + 2} - x_u^{-\alpha_\gamma + 2}} & (\alpha_\gamma \neq 2) \\ \frac{L'_\gamma}{4\pi R^2 c \varepsilon'_{\gamma 0}} \frac{1}{\ln\left(\frac{\varepsilon'_\gamma^{\max}}{\varepsilon'_\gamma^{\min}}\right)} & (\alpha_\gamma = 2), \end{cases} \quad (9)$$

where the two parameters  $x_d = (\varepsilon'_\gamma^{\min}/\varepsilon'_{\gamma 0})$  and  $x_u = (\varepsilon'_\gamma^{\max}/\varepsilon'_{\gamma 0})$  represents the boundary of the main photon emission energy range that appear in the luminosity estimation, Eq. (8). In this case, one determines the relationship between the bolometric luminosity  $L'_\gamma$  and the reference luminosity  $L'_{\gamma 0}$  [32].

The optical depth to the photo-meson production is given by (see also Eq.(6) of Ref. [33])

$$\tau_{p\gamma}(\varepsilon'_p) = \frac{2}{1 + \alpha_\gamma} \frac{L'_{\gamma 0}}{4\pi R \Gamma c \varepsilon'_{\gamma 0}} \int ds \frac{\sigma_{p\gamma}(s)}{s - m_p^2} \left( \frac{\varepsilon'_p}{\tilde{\varepsilon}'_{p0}(s)} \right)^{\alpha_\gamma - 1} \quad (10)$$

where  $\varepsilon'_p \approx \varepsilon_p/\Gamma$  and  $\sigma_{p\gamma}$  is the photo-meson production cross-section. Using the approximation  $\sigma_{p\gamma} \approx (s_\Delta - m_p^2) \bar{\sigma}_\Delta \delta(s - s_\Delta)$  (where  $\bar{\sigma}_\Delta \sim 3 \times 10^{-28} \text{ cm}^2$  is the cross-section averaged over the resonance range), we

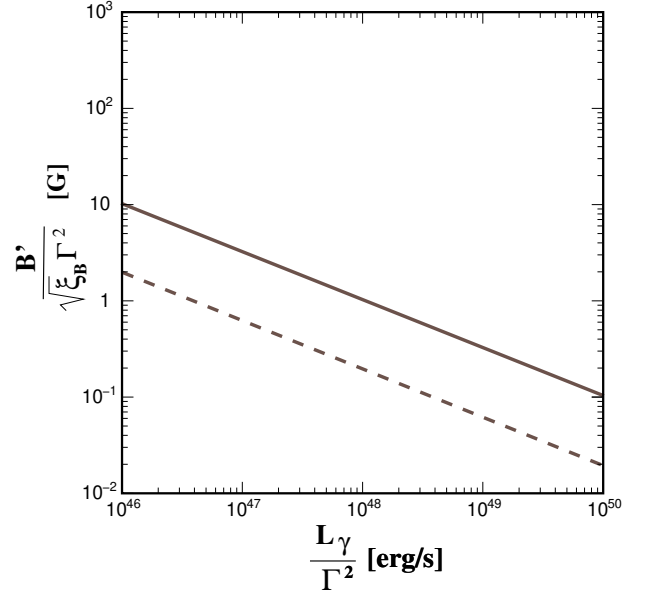


FIG. 1. The relationship between the comoving magnetic field strength  $B'$  and the comoving photon luminosity  $L'_\gamma \approx L_\gamma/\Gamma^2$ . The solid line displays the case when  $1 - \exp(-\tau_{p\gamma 0}) = 0.4$  (corresponding to  $\tau_{p\gamma 0} \sim 1$ ), which is the most optically thick case allowed by the UHECR escape condition. The dashed line shows the  $B' - L'_\gamma$  relationship when  $1 - \exp(-\tau_{p\gamma 0}) = 0.1$  (corresponding to  $\tau_{p\gamma 0} \sim 0.1$ ).

reproduce the known results (e.g., Refs. [11, 34, 35] with inelasticity taken into account). Using this resonance approximation, the preceding equation is rewritten as

$$\tau_{p\gamma}(\varepsilon_p) \approx \frac{2}{1 + \alpha_\gamma} \frac{L'_{\gamma 0}}{4\pi R \Gamma^2 c (\varepsilon'_{\gamma 0}/\Gamma)} \left( \frac{\varepsilon_p}{\tilde{\varepsilon}_{p0}^\Delta} \right)^{\alpha_\gamma - 1} \int ds \frac{\sigma_{p\gamma}(s)}{s - m_p^2} \quad (11)$$

This approximation is valid for  $\alpha_\gamma \gtrsim 1$ , and for  $\alpha_\gamma \sim 1$  there is an enhancement by a factor of 2 – 3 due to multipion production [36]. Since  $E_\nu \sim 1 \text{ PeV}$  neutrinos originate from  $\varepsilon_p \approx (1 + z)20 \text{ PeV}$  protons (where  $\bar{z}$  is the typical source redshift), we use  $\tilde{\varepsilon}_{p0}^\Delta$  as the reference proton energy (in the engine frame), which is fixed to  $\tilde{\varepsilon}_{p0}^\Delta = 10 \text{ PeV}$ . In this case, one should consider that this implicitly requires target photons that can resonantly interact with protons with an energy of 10 PeV. As such,  $\varepsilon'_{\gamma 0}$  has an implicit  $\Gamma$  dependence via Eq. (6). We have

$$\varepsilon_{\gamma 0} \approx 16 \Gamma^2 (\tilde{\varepsilon}_{p0}^\Delta / 10 \text{ PeV})^{-1} \text{ eV}. \quad (12)$$

As a result, one can see from Eq. 11 that  $\tau_{p\gamma}(\tilde{\varepsilon}_{p0}^\Delta) \equiv \tau_{p\gamma 0} \propto L_\gamma \Gamma^{-2} (\varepsilon_{\gamma 0})^{-1} R^{-1} \propto L'_\gamma \Gamma^{-1} (\varepsilon'_{\gamma 0})^{-1} R^{-1} \propto L'_\gamma \Gamma^{-2} R^{-1} \tilde{\varepsilon}_{p0}^\Delta$ .

The emission radius  $R$  appears in Eq. (11), but it can be eliminated via Eq. (2). For a given value of  $\tilde{\varepsilon}_{p0}^\Delta$ , as  $R \propto L'_\gamma / \tau_{p\gamma 0} / \Gamma^2$  and  $U'_B \propto \xi_B L'_\gamma / R^2$ , the magnetic field

strength must satisfy

$$\frac{B'/\Gamma^2}{\tau_{p\gamma 0}\sqrt{\xi_B/L'_\gamma}} = C(\alpha_\gamma, \tilde{\varepsilon}_{p0}^\Delta)^{-1}, \quad (13)$$

where  $C(\alpha_\gamma, \tilde{\varepsilon}_{p0}^\Delta)$  is a constant that depends on the photon index. For  $\bar{\sigma}_\Delta \sim 3 \times 10^{-28} \text{ cm}^2$ , we have

$$C(\alpha_\gamma, \tilde{\varepsilon}_{p0}^\Delta) \sim 2.4 \times 10^{-24} \text{ erg}^{-1} \text{ cm}^{3/2} \text{ s}^{1/2} \times \left( \frac{2}{1 + \alpha_\gamma} \right) \left( \frac{\tilde{\varepsilon}_{p0}^\Delta}{10 \text{ PeV}} \right) \left( \frac{5L'_{\gamma 0}}{L'_\gamma} \right). \quad (14)$$

The source model has been constructed such that for a given  $L'_\gamma$  and  $\Gamma$ , the  $p\gamma$  interaction site radius  $R$  can arbitrarily vary to realize various values of  $\tau_{p\gamma 0}$  and  $B'$  (assuming a value of the equipartition parameter  $\xi_B$ ) via Eqs. (11) and (2). This enables us to eliminate the model dependence on  $R$  that is often very uncertain (see Refs. [36, 37] for GRBs). Eq. (13) can further be combined with the conditions for UHECR acceleration and survival. The explicit independent parameters for this construction are then  $L'_\gamma$ ,  $\Gamma$ , and  $\tau_{p\gamma 0}$ , as well as the sub-parameters  $\xi_B$  and  $\alpha_\gamma$ .

With Eqs. (4) and (13), one of the UHECR acceleration conditions gives the following upper limit on the  $p\gamma$  optical depth:

$$\tau_{p\gamma 0} < \frac{C(\alpha_\gamma, \tilde{\varepsilon}_{p0}^\Delta) 6\pi e m_p^4 c^4 A^4}{\sigma_T m_e^2} \frac{A^4}{Z^3} \left( \frac{L'_\gamma{}^{1/2}}{\xi_B^{1/2} (\varepsilon_i^{\max})^2} \right). \quad (15)$$

By applying the UHECR escape condition (5) to the optical depth formula, Eq. (11), we can obtain the condition for  $\tau_{p\gamma 0}$  without explicitly depending on  $L'_\gamma$  and  $\Gamma$  as:

$$\tau_{p\gamma 0} < \frac{2}{1 + \alpha_\gamma} \left( \int ds \frac{\sigma_{p\gamma}}{s - m_p^2} \right) \frac{3A^4 m_p^4 c^4 (L'_{\gamma 0}/L'_\gamma)}{4Z^4 \sigma_T m_e^2 (\varepsilon'_{\gamma 0}/\Gamma)} \frac{1}{\xi_B \varepsilon_i^{\max}} \lesssim 6 \times 10^{-2} \frac{2}{1 + \alpha_\gamma} \xi_B^{-1} \left( \frac{A}{Z} \right)^4 \left( \frac{\varepsilon_i^{\max}}{10^{11} \text{ GeV}} \right)^{-1} \quad (16)$$

It should be noted that  $\varepsilon'_{\gamma 0}/\Gamma = (s_\Delta - m_p^2)/4\tilde{\varepsilon}_{p0}^\Delta$  and thus, this bound is  $\Gamma$  independent.

Fig. 1 displays this dependence for two representative cases for  $\tau_{p\gamma 0}$  – the optical depth of protons with energy  $\tilde{\varepsilon}_{p0}^\Delta = 10 \text{ PeV}$ .

It should be noted that the UHECR acceleration and survival conditions require that  $t'_{\text{acc}} < t'_{p\gamma}$  and  $t'_{\text{dyn}} < t'_{p\gamma}$  should also be satisfied. The latter condition means that the system should not be calorimetric to the sources to simultaneously account for the IceCube neutrino and UHECR fluxes. Therefore, we have

$$\tau_{p\gamma 0} \leq \tau_{p\gamma}(\varepsilon_p^{\max}) \lesssim 1/\kappa_{p\gamma} \sim 5, \quad (17)$$

where  $\kappa_{p\gamma} \sim 0.2$  is the proton inelasticity. In the cases whereby  $\alpha_{\text{cr}} \geq 2$ , this condition is satisfied by the diffuse flux measurements (see below), so that  $t_{\text{acc}} < t_{\text{dyn}} < t_{p\gamma}$  is automatically fulfilled.

### III. CONSTRAINTS DUE TO DIFFUSE UHECR AND NEUTRINO FLUXES

An important observation is that the energy generation rate densities of UHECRs and neutrinos are comparable [7, 38]. The detailed comparison of these fluxes constrains the parameter space of the unification model.

#### A. Neutrino spectra with radiative cooling of mesons and muons

The flux of high-energy neutrinos for a given optical depth  $\tau_{p\gamma 0}$  has been calculated using various analytical and numerical methods. In this work, based on Ref. [33], we outline the analytical formulation and its minor modifications to account for the synchrotron cooling of mesons and muons.

The spectrum of UHECRs injected from the UHECR sources is assumed to follow a power-law form, which is

$$\frac{d\dot{N}_{\text{CR}}}{d\varepsilon_i} = \frac{K_{\text{CR}}}{\varepsilon_{i0}} \left( \frac{\varepsilon_i}{\varepsilon_{i0}} \right)^{-\alpha_{\text{CR}}} e^{-\varepsilon_i/\varepsilon_i^{\max}}, \quad (18)$$

where  $\varepsilon_{i0}$  is the reference energy that can be set to  $\tilde{\varepsilon}_{p0}^\Delta$  for protons. The normalization factor,  $K_{\text{CR}}$ , of the UHECR yield (with a dimension of  $[\text{s}]^{-1}$ ) is linked quasibolometrically to the photon luminosity  $L_\gamma$  with the CR loading factor  $\xi_{\text{CR}}$ :

$$K_{\text{CR}} \approx \begin{cases} \frac{(\alpha_{\text{CR}} - 2)\xi_{\text{CR}} L_\gamma / \varepsilon_{i0}}{\left(\frac{\varepsilon_i^{\min}}{\varepsilon_{i0}}\right)^{-\alpha_{\text{CR}} + 2} - \left(\frac{\varepsilon_i^{\max}}{\varepsilon_{i0}}\right)^{-\alpha_{\text{CR}} + 2}} & (\alpha_{\text{CR}} \neq 2) \\ \frac{\xi_{\text{CR}} L_\gamma / \varepsilon_{i0}}{\ln\left(\frac{\varepsilon_i^{\max}}{\varepsilon_i^{\min}}\right)} & (\alpha_{\text{CR}} = 2). \end{cases} \quad (19)$$

Assuming that UHECRs are protons, we set  $\varepsilon_i^{\min} = \tilde{\varepsilon}_{p0}^\Delta = 10 \text{ PeV}$  hereafter.

In general, if pions and muons decay into gamma rays and leptons without energy loss, the differential neutrino luminosity from a single source,  $d\dot{N}_\nu/d\varepsilon_\nu$  is formally given by [26, 39]

$$\frac{d\dot{N}_\nu}{d\varepsilon_\nu} \approx \int d\varepsilon_i \frac{d\dot{N}_{\text{CR}}}{d\varepsilon_i} \int d\varepsilon'_\gamma \frac{dn_\gamma}{d\varepsilon'_\gamma} \left\langle \frac{d\sigma_{p\gamma \rightarrow \nu}}{d\varepsilon_\nu}(\varepsilon_i, \varepsilon'_\gamma) \right\rangle ct'_{\text{cool}}, \quad (20)$$

where  $d\sigma_{p\gamma \rightarrow \nu}/d\varepsilon_\nu$  is the inclusive differential cross-section with the multiplicity of neutrinos taken into account. Given that we focus on  $t'_{\text{cool}} \approx t'_{\text{dyn}}$ , with the energy dependent optical depth  $\tau_{p\gamma} \approx$

$\int d\varepsilon'_\gamma (dn_\gamma/d\varepsilon'_\gamma) \langle \sigma_{p\gamma} \rangle ct'_{\text{dyn}}$ , the preceding equation is approximated to be [33]

$$\frac{d\dot{N}_\nu}{d\varepsilon_\nu} \approx \int d\varepsilon_i \frac{K_{\text{CR}}}{\varepsilon_{i0}} \left( \frac{\varepsilon_i}{\varepsilon_{i0}} \right)^{-\alpha_{\text{CR}}} Y(\varepsilon_\nu; \varepsilon_i) \tau_{p\gamma}(\varepsilon_i). \quad (21)$$

In this case,  $Y(\varepsilon_\nu; \varepsilon_i)$  denotes the energy distribution of the neutrinos produced by an interaction of a cosmic ray proton. The details of the expression for  $Y$  are given in Appendix A (see also Refs. [40, 41] for another analytical approximation). It should be noted that the neutrino spectrum cannot be harder than  $\propto \varepsilon_\nu^0$  [35, 42].

The radiative cooling of pions and muons is important when the cooling time becomes “shorter” than the decay time [11, 43], provided that their escape time from the turbulent magnetic field region is much longer. In general, various processes such as inverse Compton and adiabatic losses can be relevant. We consider the case of synchrotron dominance. The ratio of the synchrotron cooling time to the decay time can be written as

$$\frac{t'_{\pi/\mu, \text{syn}}}{t'_{\pi/\mu, \text{dec}}} = \left( \frac{\varepsilon_{\nu, \pi/\mu}^{\text{syn}}}{\varepsilon_\nu} \right)^2, \quad (22)$$

where  $t'_{\pi/\mu, \text{syn}}$  is the synchrotron time scale of pions (muons),  $t'_{\pi/\mu, \text{dec}} = [\varepsilon'_{\pi/\mu}/(m_{\pi/\mu}c^2)]\tau_{\pi/\mu}$  is the lifetime of pions and muons, and  $\tau_{\pi/\mu}$  is their proper lifetime. In addition,  $\varepsilon_{\nu, \pi/\mu}^{\text{syn}}$  is the critical neutrino energy of a pion (or muon), above which the suppression due to synchrotron cooling is relevant. The critical energy is given by [11, 44]

$$\varepsilon_{\nu, \pi/\mu}^{\text{syn}} \approx \Gamma \kappa_{\pi, \mu} \sqrt{\frac{6\pi}{\tau_{\pi, \mu} \sigma_T c B'^2} \frac{(m_{\pi/\mu}c^2)^5}{(m_e c^2)^2}}, \quad (23)$$

where  $\kappa_{\pi, \mu}$  is the inelasticity from pion (muon) to a neutrino in the decay process. In this work,  $\kappa_\pi$  is approximated by  $\sim 1 - r_\pi$  [42], where  $r_\pi = m_\mu^2/m_\pi^2 \approx 0.57$  is the muon-to-pion mass-squared ratio. The other fraction goes to a muon and  $\kappa_\mu$  is approximated as  $\sim 0.3$ .

In the synchrotron cooling energy regime, *i.e.*,  $\varepsilon_\nu \geq \varepsilon_{\nu}^{\text{syn}}$ , the neutrino yield is suppressed by  $t'_{\pi/\mu, \text{syn}}/t'_{\pi/\mu, \text{dec}}$ . Introducing  $f_{\text{sup}}(\varepsilon_\nu) = 1 - \exp(-t'_{\pi/\mu, \text{syn}}/t'_{\pi/\mu, \text{dec}})$  [40, 41], the neutrino yield, Eq. (20), is modified as

$$\frac{d\dot{N}_\nu}{d\varepsilon_\nu} \approx \int d\varepsilon_i \frac{K_{\text{CR}}}{\varepsilon_{i0}} \left( \frac{\varepsilon_i}{\varepsilon_{i0}} \right)^{-\alpha_{\text{CR}}} \tau_{p\gamma}(\varepsilon_i) Y(\varepsilon_\nu; \varepsilon_i) f_{\text{sup}}(\varepsilon_\nu) \quad (24)$$

The break energy of the neutrino flux due to synchrotron cooling is given by Eq.(23) and scales as  $\varepsilon_{\nu}^{\text{syn}} \propto \Gamma R/\sqrt{L'_\gamma}$ . Since the optical depth  $\tau_{p\gamma 0}$  scales as  $\propto L'_\gamma/(R\Gamma^2)$ , we get  $\varepsilon_{\nu}^{\text{syn}} \propto \sqrt{L'_\gamma}/(\Gamma\tau_{p\gamma 0})$ . Thus, the upper limit of the neutrino flux in the energy region beyond 10 PeV for IceCube [45] can constrain  $L'_\gamma$ ,  $\Gamma$  and  $\tau_{p\gamma 0}$ .

## B. Calculations of diffuse intensities

Assuming emission from standard candles (*i.e.*, identical sources over redshifts), the energy flux of diffuse neutrinos from UHECR sources across the universe,  $\Phi_\nu \equiv dJ_\nu/dE_\nu$ , is calculated by (*e.g.*, [35])

$$E_\nu^2 \Phi_\nu(E_\nu) = \frac{c}{4\pi} \int_0^{z_{\text{max}}} \frac{dz}{1+z} \left| \frac{dt}{dz} \right| \left[ \varepsilon_\nu^2 \frac{d\dot{N}_\nu}{d\varepsilon_\nu}(\varepsilon_\nu) \right] n_0 \psi(z), \quad (25)$$

where  $d\dot{N}_\nu/d\varepsilon_\nu$  is the neutrino spectrum per source, which is calculated in the previous subsection, and  $E_\nu = \varepsilon_\nu/(1+z) \approx \Gamma\varepsilon'_\nu/(1+z)$ . The comoving number density of UHECR sources is represented by  $n_0\psi(z)$  with the local source density at  $z=0$ ,  $n_0$ , and its cosmological evolution factor  $\psi(z)$ . For transient sources such as GRBs,  $n_0$  is effectively given by  $n_0 = \rho_0\Delta T$ , where  $\rho_0$  and  $\Delta T$  are the rate density and the duration of neutrino emission at the sources.

The evolution factor  $\psi(z)$  is parameterized as  $(1+z)^m$  such that the parameter  $m$  represents the “scale” of the cosmological evolution that is often used in the literature. In this work, the source evolution is assumed to be compatible with the star formation rate, which is consistent with the constraints on cosmogenic neutrinos with extremely-high energy (EHE) analysis by IceCube [46]. Following Refs. [47, 48], we parameterize  $\psi(z)$  as

$$\psi(z) \propto \begin{cases} (1+z)^{3.4} & (0 \leq z \leq 1) \\ \text{constant} & (1 \leq z \leq 4) \end{cases}. \quad (26)$$

Based on Eq. (17),  $\varepsilon_i^2(d\dot{N}_{\text{CR}}/d\varepsilon_i)$  can essentially be regarded as the luminosity of injected cosmic rays. Then,  $n_0\varepsilon_i^2(d\dot{N}_{\text{CR}}/d\varepsilon_i)$  corresponds to the UHECR luminosity density that is known to be  $E_i(dQ_{\text{CR}}/dE_i) \approx 10^{43.8}$  erg Mpc<sup>-3</sup> yr<sup>-1</sup> [7, 38]. The diffuse neutrino flux measurements suggest that the energy generation rate density of neutrinos is comparable,  $E_\nu(dQ_\nu/dE_\nu) \approx 10^{43.3}$  erg Mpc<sup>-3</sup> yr<sup>-1</sup> [38]. Both the UHECR and the neutrino diffuse fluxes scale as  $\propto n_0\varepsilon_{i0}K_{\text{CR}} \sim n_0\xi_{\text{CR}}L_\gamma \approx n_0\xi_{\text{CR}}L'_\gamma\Gamma^2$ . It is convenient to introduce the *boosted* source number density defined as

$$\begin{aligned} \mathcal{N}_\Gamma &\equiv n_0\xi_{\text{CR}}\Gamma^2 \\ &= \rho_0\Delta T\xi_{\text{CR}}\Gamma^2. \end{aligned} \quad (27)$$

The UHECR and neutrino intensities are then proportional to  $\mathcal{N}_\Gamma$  for a given comoving photon luminosity  $L'_\gamma$ . It should be noted that  $Q_{\text{CR}}(> 10 \text{ PeV}) = L'_\gamma\mathcal{N}_\Gamma = \xi_{\text{CR}}L_\gamma n_0$ . The full description of  $\Phi_\nu$  with the present analytical formulation is given in Appendix A.

Fig. 2 shows an example of the UHECR and neutrino fluxes derived using the presented generic model. This realization of the fluxes displayed in Fig. 2 is associated with a scenario that is consistent with the UHECR

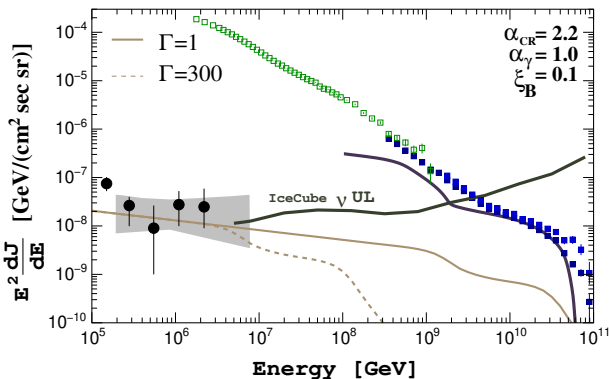


FIG. 2. An example of the UHECR nucleon and the all-flavor-sum neutrino fluxes from UHECR sources calculated using the presented analysis. The case of  $\alpha_{\text{CR}} = 2.2$ ,  $\alpha_{\gamma} = 1.0$ ,  $\xi_{\text{B}} = 0.1$  is shown, assuming star formation rate-like evolution. The co-moving  $L'_{\gamma}$  is set to  $4.5 \times 10^{46}$  erg/s and the boosted source number density  $\mathcal{N}'_{\Gamma}$  (Eq. 27) is  $1 \times 10^{-9}$  Mpc $^{-3}$ . The optical depth  $\tau_{p\gamma 0}$  is 0.30 in this example, which gives a magnetic field of  $B' = 0.91\Gamma^2$  G with  $\xi_{\text{B}} = 0.1$ . The black points represent the IceCube neutrino measurements [49] and the shaded region represents the flux space, consistent with the IceCube diffuse  $\nu_{\mu}$  data [4]. The solid curve labeled as (IceCube  $\nu$  UL) is the differential EHE bound for IceCube [45]. The cosmic ray data measured by IceTop [50], PAO [51] and TA [52] are also displayed.

and IceCube data. We discuss the allowed parameter space in the next section. It should be noted that the  $1/\Gamma$  dependence of the neutrino cut-off energy due to the pion/muon synchrotron losses is also observed in this plot.

The spectrum of the UHECR protons after their propagation through intergalactic space to reach the Earth is calculated using a similar analytical technique. The details will be described in Appendix B.

### C. Observational constraints

The predicted neutrino and UHECR spectra must be consistent with their observations. Qualitatively, the UHECR energy budget constrains the product of  $L'_{\gamma}$  and  $\mathcal{N}'_{\Gamma}$ , whereas the neutrino energy budget determines the product of  $\tau_{p\gamma 0}$  and  $L'_{\gamma}\mathcal{N}'_{\Gamma}$ . To quantify this consistency, we introduce the following criteria in the present study.

- The integrated UHECR proton flux above 10 EeV,  $\int_{10\text{EeV}} dE_i dJ_{\text{CR}}/dE_i$ , is less than the measurement by Auger,  $8.5 \times 10^{-19}$  /cm $^2$ /s/sr [51]. Considering the uncertainties associated with the UHECR mass composition, we only request these bolometric requirements of the UHECR flux to be conservative with respect to imposing bounds on the relevant parameter space. The results for the required UHECR energy generation rate density are consis-

tent with those obtained based on detailed numerical simulations considering the uncertainties.

- The neutrino flux intensity at 100 TeV and the spectral power law index are within the 99 % C.L. range obtained by the diffuse  $\nu_{\mu}$  data measured by IceCube [4].
- The all-flavor-sum neutrino flux at 100 PeV is less than  $2 \times 10^{-8}$  GeV/cm $^2$ /s/sr, the limit obtained by the IceCube EHE analysis [45].
- The neutrino flux at 6 PeV is above  $2 \times 10^{-9}$  GeV/cm $^2$ /s/sr, determined by the 6 PeV energy neutrino detection by IceCube [45].

## IV. CONSTRAINTS ON UHECR AND NEUTRINO EMITTERS

Four constraints from UHECR acceleration (Eqs. 1 and 15), UHECR escape (Eqs. 16 and 17) based on the physics of photo-meson production, and diffuse UHECR and neutrino flux measurements, allow us to constrain generic unification models for photohadronic neutrinos. We present the results in the following.

### A. Cases of fiducial neutrino spectra

The left plot of Fig. 3 displays the luminosity and the optical depth constraints for the spectral power law index of UHECRs  $\alpha_{\text{CR}} = 2.2$  and that of the target photons  $\alpha_{\gamma} = 1.0$ . Given that the neutrino spectrum follows  $\propto E_{\nu}^{-(\alpha_{\text{CR}} - \alpha_{\gamma} + 1)} \sim E_{\nu}^{-2.2}$  (see Eq. (A3)), they represent the case of neutrino spectra with  $\alpha_{\nu} > 2$ , which is close to the index suggested by IceCube observations. The optical depth  $\tau_{p\gamma 0} \gtrsim 0.1$  is required because the IceCube neutrino energy flux is compatible with the UHECR flux. As seen in Fig. 2, the margins for the neutrino fluxes to be consistent with both the neutrino and UHECR observations are small when the primary UHECR spectrum is as hard as  $\alpha_{\text{CR}} \lesssim 2.2$ . Since  $L'_{\gamma}\mathcal{N}'_{\Gamma} \propto n_0 K_{\text{CR}}$ , the range of the luminosity per unit volume,  $L'_{\gamma}\mathcal{N}'_{\Gamma}$ , is bounded by the UHECR flux and the IceCube neutrino flux connected by the optical depth  $\tau_{p\gamma 0}$ . This is an expanded way of presenting the bounds leading to the frequently referenced Waxman-Bahcall limit [53]. The tight constraint is also consistent with the results in Ref. [33]. The resultant range of the source luminosity per unit volume is  $\sim (3 - 15) \times 10^{44}$  erg Mpc $^{-3}$  yr $^{-1}$ . This is comparable with the integrated UHECR luminosity per unit volume at  $z = 0$  above  $10^{18}$  eV [54].

However, the UHECR escape condition, Eq. (16), prevents large optical depths unless the magnetic field is weaker than expected from the equipartition condition  $\xi_{\text{B}} = 1$ . The bound of  $\tau_{p\gamma 0} \lesssim 0.06$  derived by Eq. (16) with the equipartition condition  $\xi_{\text{B}} = 1$  is obviously inconsistent with the shaded region in the left plot of Fig. 3.

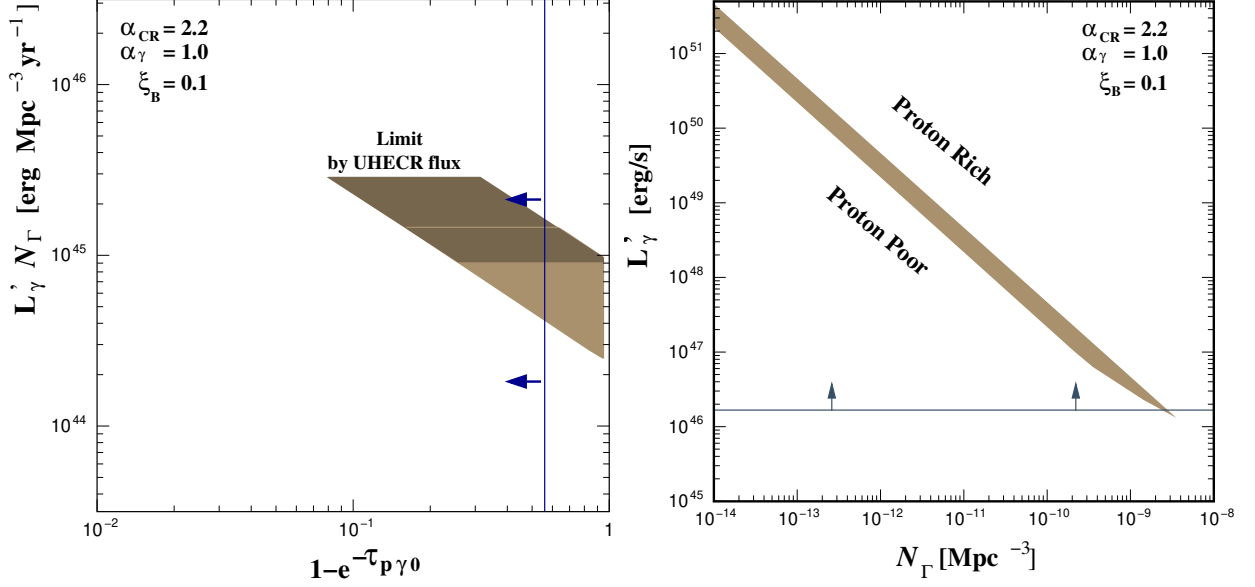


FIG. 3. (Left) The allowed region in the parameter space of luminosity per unit volume,  $L'_\gamma N_\Gamma$ , and damping factor  $1 - e^{-\tau_{p\gamma 0}}$ . The parameters inside the shaded region satisfy the observational consistency criteria of conditions (a)~(d) described in the text, and the UHECR condition of Eq. (15). The cases of  $\alpha_{CR} = 2.2$  and  $\gamma = 1.0$  are shown. We find no  $\Gamma$  dependence on these constraints. The horizontal belt represented by the darker shade shows the systematics of the UHECR energetics that originate from the uncertainties on the mass composition and Galactic to the extragalactic transition of UHECRs [38]. The vertical line represents the bound on  $\tau_{p\gamma 0}$  by the UHECR escape condition, Eq. (16) when  $\xi_B = 0.1$ . The maximal bound of  $L'_\gamma N_\Gamma$  is determined by the condition whereby the proton flux from sources should not exceed the measured flux of UHECRs. The lower bound is driven by the intensity of neutrinos measured by IceCube. (Right) The allowed region on the plane of the source luminosity  $L'_\gamma$  and the boosted source density  $N_\Gamma$ . The parameters inside the shaded region satisfy the observational consistency criteria as shown in the left plot. The horizontal line represents the condition of  $t_p^{\text{acc}} \leq t_p^{\text{dyn}}$ , Eq. (1).

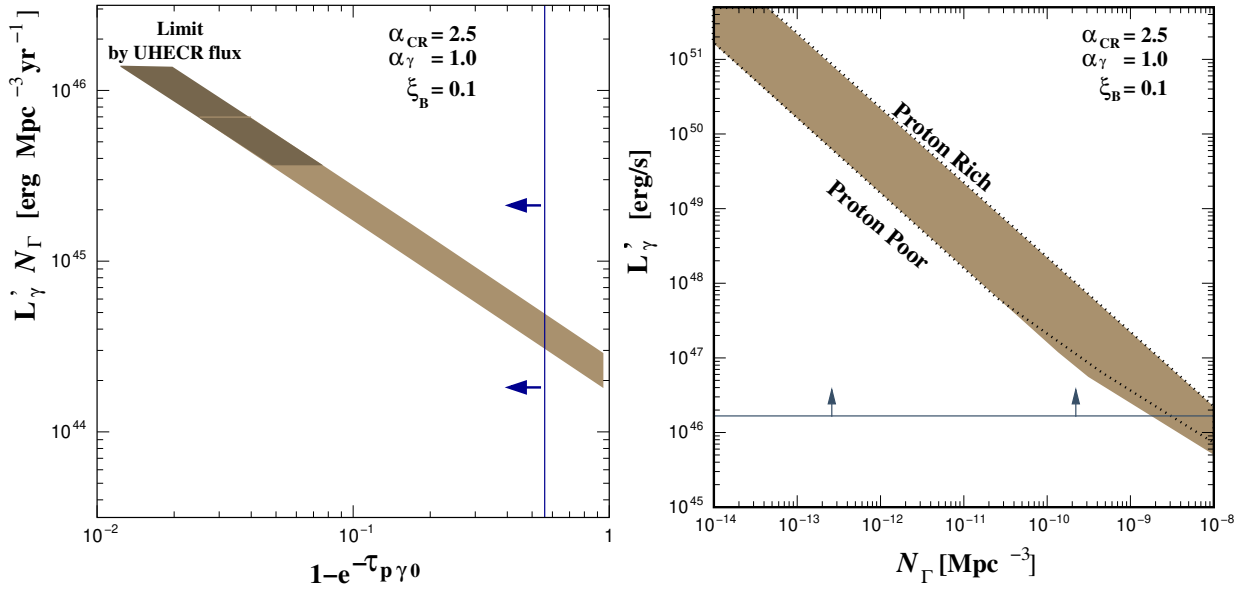


FIG. 4. Same as Fig. 3 but for  $\alpha_{CR} = 2.5$ . The constraints on  $L'_\gamma - N_\Gamma$  (right) has a small dependence on  $\Gamma$  when  $\Gamma \gg 1$ . The region specified by the dashed line corresponds to the allowed space for  $\Gamma = 100$ .

Relaxation of the criteria for proton synchrotron cooling by setting  $\xi_B \sim 0.1$  can open an allowed space of the parameters,  $L'_\gamma \mathcal{N}_\Gamma$  and the optical depth  $\tau_{p\gamma 0}$ . We found that the cases of even harder UHECR source spectrum, *i.e.*,  $\alpha_{\text{CR}} \lesssim 2.1$  is nearly excluded for a reasonable range of the magnetic field strengths that are expected due to  $\xi_B \gtrsim 0.1$ . Given that the upper bound of  $\tau_{p\gamma 0}$  required by the UHECR escape condition scales as  $1/\varepsilon_i^{\text{max}}$ , (*c.f.* Eq. (16)), setting  $\varepsilon_i^{\text{max}} \ll 10^{11}$  GeV relaxes these constraints.

We also found that the allowed range of optical depths is limited, yielding  $0.1 \lesssim \tau_{p\gamma 0} \lesssim 0.6$  for a given value of  $\xi_B \sim 0.1$ , and it is even more severely constrained if  $\xi_B \gg 0.1$ . This is nearly a universal bound regardless of the UHECR spectral index if  $\alpha_{\text{CR}} \lesssim 2.3$ .

The right plot of Fig. 3 shows the allowed parameter space on the source luminosity in the plasma rest frame  $L'_\gamma$  and the boosted source number density  $\mathcal{N}_\Gamma$ . For the requirement of the luminosity condition, Eq. 1, the unified sources must be relatively rare,  $\mathcal{N}_\Gamma \lesssim 10^{-9}$  Mpc $^{-3}$ . This is a well-known consequence of the UHECR energy budget argument. The minimal value of  $L'_\gamma$  in the shaded region is determined by the synchrotron cooling condition,  $t'_{\text{acc}} < t'_{\text{syn}}$ , Eq. (15), but the lower bound of  $L'_\gamma$  demanding  $t'_{\text{acc}} < t'_{\text{dyn}}$ , Eq. (1), is more stringent.

We note that these constraints in the plane of luminosity per unit volume and the optical depth, and the plane of  $L'_\gamma$ - $\mathcal{N}_\Gamma$  are nearly independent of the plasma bulk Lorentz factor  $\Gamma$ . Thus, they are universal conditions that any class of sources in a unification scheme should satisfy.

The constraints on the source luminosity per unit volume  $L'_\gamma \mathcal{N}_\gamma$  can be relaxed for the case of the *soft* UHECR (and thus neutrino) spectra. Fig. 4 displays an example,  $\alpha_{\text{CR}} = 2.5$ . Since the margin between UHECR and the neutrino fluxes increases if the UHECR proton spectrum is steeper, the luminosity per volume can be  $\gtrsim 3 \times 10^{45}$  erg Mpc $^{-3}$  yr $^{-1}$ . The sources that satisfy this requirement for CRs include galaxies, AGNs, and, galaxy clusters [38].

## B. Cases of hard neutrino spectra

Although cases of harder UHECR spectra, *i.e.*,  $\alpha_{\text{CR}} \lesssim 2.1$  are nearly eliminated, a scenario that predicts hard *neutrino* spectra with  $\alpha_\nu \lesssim 2.0$  is more realistic if the target photon spectrum is softer as  $\alpha_\gamma \gtrsim 1.3$ . It should be noted that the neutrino spectrum follows  $\sim E_\nu^{-(\alpha_{\text{CR}} - \alpha_\gamma + 1)}$  according to Eq. (A3). A hard neutrino spectrum like  $\sim E_\nu^{-2}$  cannot extend well above 100 PeV and should attenuate at a point below this value, given that the spectral extension to  $\gg$  PeV with a  $E_\nu^{-2}$ -like power-law flux has been eliminated by the IceCube EHE limit (see Fig. 3 of Ref. [46]). The spectral fall-off behavior of the neutrino spectrum is naturally expected when strong synchrotron cooling occurs. As discussed earlier, since the characteristic synchrotron cut-off en-

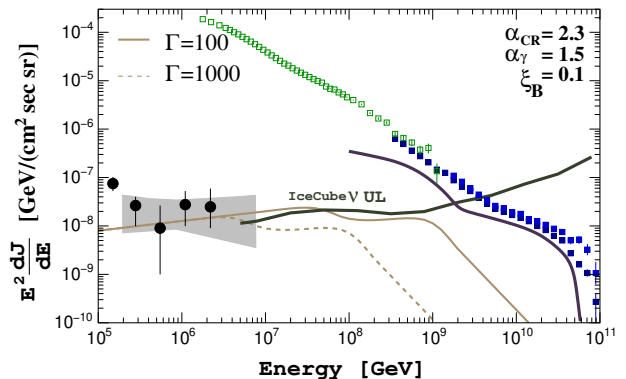


FIG. 5. An example of scenario for hard neutrino flux.  $\alpha_{\text{CR}} = 2.3$  and  $\alpha_\gamma = 1.5$ . The comoving  $L'_\gamma$  is set to  $5.0 \times 10^{48}$  erg/s and the boosted source number density  $\mathcal{N}_\Gamma$  (Eq. 27) is  $1 \times 10^{-9}$  Mpc $^{-3}$ . The optical depth  $\tau_{p\gamma 0}$  is 0.10 in this particular example, we have a magnetic field of  $B' = 0.26\Gamma^2$  G with  $\xi_B = 0.1$ .

ergy of neutrinos is  $\varepsilon_\nu^{\text{syn}} \sim \sqrt{L'_\gamma}/(\Gamma\tau_{p\gamma 0})$ , a lower energy cut-off via synchrotron cooling is realized in relativistic plasma flow *i.e.*,  $\Gamma \gg 1$ . A scenario of harder neutrino spectra (but softer UHECR spectra) is, therefore, a natural consequence of the unified UHECR/neutrino model for ultra-relativistic sources.

An example of the ultra-relativistic scenario is shown in Fig. 5. The hard neutrino spectrum  $\propto E_\nu^{-(\alpha_{\text{CR}} - \alpha_\gamma + 1)} \sim E_\nu^{-1.8}$  falls off at  $\sim 500$  (50) PeV for sources with  $\Gamma = 100$  (1000). These spectra are consistent with the IceCube EHE limit [45] based on the null detection of  $\gtrsim 10$  PeV neutrinos. They represent a scenario of ultra-relativistic sources with unified UHECR and neutrino emission.

Since the cut-off energy of the neutrino spectrum depends explicitly on  $\Gamma$  for a given optical depth, the constraints on  $L'_\gamma$ ,  $\mathcal{N}_\gamma$ , and  $\tau_{p\gamma 0}$  exhibits a weak dependence on  $\Gamma$  in the case of extremely relativistic sources that yield hard neutrino fluxes. Fig. 6 displays the allowed region of parameter spaces in the hard neutrino spectrum. Since  $E_\nu^{\text{syn}} \propto \sqrt{L'_\gamma}/(\Gamma\tau_{p\gamma 0})$ , a lower  $\Gamma$  excludes super-luminous sources, because the neutrino intensity at  $\gg$  PeV would overshoot the IceCube EHE limit.

Given that the spectral indexes  $\alpha_{\text{CR}}$  and  $\alpha_\gamma$  characterize the emission environments, it is important to understand their allowed space in the unified source model. Fig. 7 shows the constraints in the plane of  $\alpha_{\text{CR}}$  and  $\Gamma$  for various values of the photon spectral power-law index  $\alpha_\gamma$ . The rapid fall-off structures observed at  $\Gamma \sim 20$  result from the spectral cut-off due to synchrotron cooling. A higher  $\Gamma$  facilitates larger parameter spaces of  $\alpha_{\text{CR}}$  and  $\alpha_\gamma$  as it avoids the EHE neutrino limit. The figure also indicates that extremely relativistic cases,  $\Gamma \sim 10^3$ , would further extend the allowed parameter space. This is because strong synchrotron cooling softens a fairly hard spectrum of neutrinos, which would otherwise be incon-



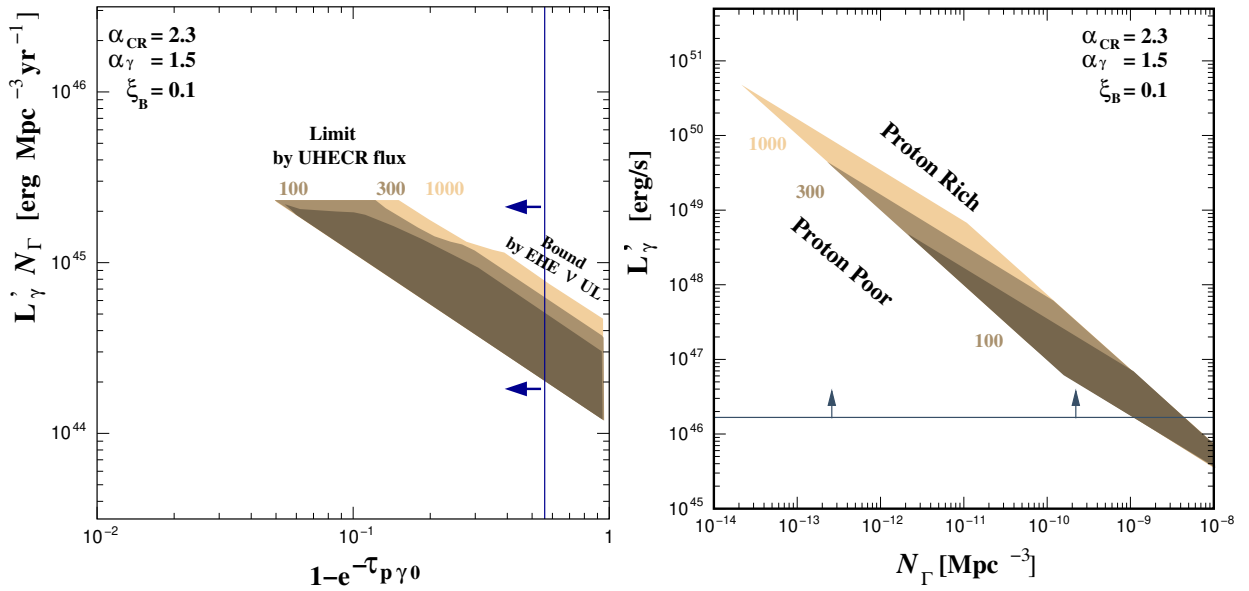


FIG. 6. Same as Fig. 3 but with  $\alpha_{\text{CR}} = 2.3$  and  $\alpha_\gamma = 1.5$ . Only a relativistic plasma flow,  $\Gamma \gtrsim 30$ , can be consistent with the observation and the resultant allowed region has weak dependences on  $\Gamma$ . In these plots, the allowed parameter space for  $\Gamma = 100$ ,  $\Gamma = 300$ , and  $\Gamma = 1000$  are represented using different shades.

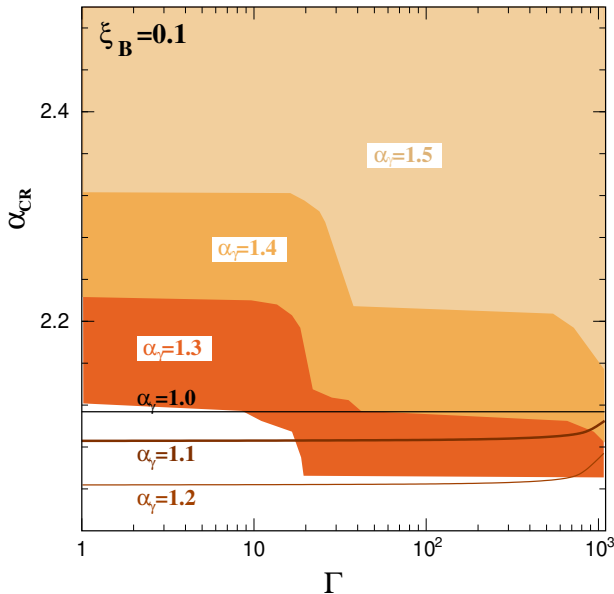


FIG. 7. The allowed region in the plane of  $\alpha_{\text{CR}}$  and  $\Gamma$ . The regions for  $\alpha_\gamma = 1.4$  and  $\alpha_\gamma = 1.3$  and  $\alpha_\gamma = 1.5$  are represented by different shades. The cases of  $\alpha_\gamma = 1.0$ ,  $1.1$ , and  $1.2$  are represented by the solid curve. The region above each of the lines is allowed.  $\xi_B = 0.1$  is assumed.

sistent with the IceCube observation.

Fig. 7 also indicates that harder UHECR proton emission  $\alpha_{\text{CR}} \lesssim 2.1$  is nearly excluded, as discussed earlier. This bound depends on the photon spectral index  $\alpha_\gamma$  in a non-trivial way. The situation is illustrated in Fig. 8.

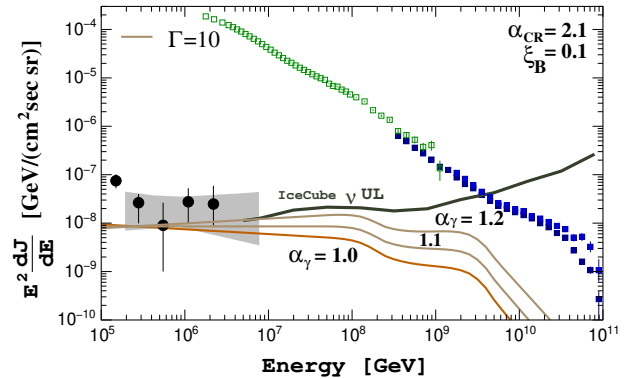


FIG. 8. An example of neutrino energy spectra from the hard UHECR flux with  $\alpha_{\text{CR}} = 2.1$ . In this example,  $L'_\gamma$ ,  $N_\Gamma$ , and  $\tau_{p\gamma 0}$  are  $8.4 \times 10^{46}$  erg s $^{-1}$ ,  $3.0 \times 10^{-10}$  Mpc $^{-3}$ , and  $0.42$ , respectively, which give a magnetic field of  $B' = 0.91\Gamma^2$  G with  $\xi_B = 0.1$ . The case of  $\alpha_\gamma = 1.0$  is not consistent with the IceCube diffuse  $\nu_\mu$  analysis [4].

The cases of  $\alpha_\gamma = 1.1$  and  $1.2$  are allowed but  $\alpha_\gamma = 1.0$  is inconsistent because it is too soft to be allowed in the diffuse  $\nu_\mu$  observations (condition (b) described in Sec. II A). The IceCube data favors a harder spectrum when we assume a lower side of the allowed intensity region  $E_\nu^2/dJ_{\nu_e+\nu_\mu+\nu_\tau}/dE_\nu \sim 1 \times 10^8$  GeV cm $^{-2}$  s $^{-1}$  sr $^{-1}$  which is the only possibility that allows for consistency with the UHECR flux.

### C. Cases of UHECR nuclei

The recent observations by Auger indicate that UHECRs are likely to have a mixed composition that is dominated by intermediate to heavy nuclei at the highest energies. This adds important conditions to the possible classes of the sources. That is, we require that nuclei with  $A > 1$  and  $Z > 1$  are accelerated and survive. The maximum proton energy can be lower, but the survival conditions constrain the source environments more strongly as investigated for GRBs [37, 55] and AGNs [25, 56].

The luminosity requirement (Eq. 1) is significantly relaxed in the cases of heavy nuclei. The condition by  $t_{\text{acc}} < t_{\text{syn}}$  is similarly imposed via Eq. (15). The new requirements originate from the photodisintegration of nuclei. As in the proton case, we focus on the situation wherein the system is effectively optically thin to photodisintegration and photo-meson production, in which  $t'_{\text{acc}} < t'_{\text{dis}}$  is automatically satisfied. In this case,  $t'_{\text{dis}}$  is the photodisintegration energy loss time.

After the nuclei are accelerated, they must survive photodisintegration while they leave the sources. The survival condition is more severe [37, 57]. The photodisintegration cross-section is larger than that for photo-meson production, which gives the optical depth:

$$\tau_{A\gamma}(\varepsilon_i) \approx \frac{2}{1 + \alpha_\gamma} \frac{L'_{\gamma 0}}{4\pi R \Gamma c \varepsilon'_{\gamma 0}} \left( \int ds \frac{\sigma_{A\gamma}(s)}{s - m_A^2} \right) \left( \frac{\varepsilon_i}{\tilde{\varepsilon}_{i0}^{\text{GDR}}} \right)^{\alpha_\gamma - 1} \quad (28)$$

where  $\tilde{\varepsilon}_{i0}^{\text{GDR}}$  is introduced as

$$\begin{aligned} \tilde{\varepsilon}_{i0}^{\text{GDR}} &= \frac{s_{\text{GDR}} - m_A^2}{4} \frac{\Gamma}{\varepsilon'_{\gamma 0}} \\ &= \frac{s_{\text{GDR}} - m_A^2}{s_\Delta - m_p^2} \tilde{\varepsilon}_{p0}^\Delta, \end{aligned} \quad (29)$$

where  $s_{\text{GDR}} = m_A^2 + 2m_A \bar{\varepsilon}_{\text{GDR}}$  is the Mandelstam variable at the giant dipole resonance, where  $\bar{\varepsilon}_{\text{GDR}} \approx 42.65 A^{-0.21}$  MeV is the resonance energy. The photodisintegration process is dominated by the giant dipole resonance. This relates  $\tau_{A\gamma}$  to  $\tau_{p\gamma}$  as

$$\tau_{p\gamma 0} \approx \tau_{A\gamma}(\varepsilon_i^{\text{max}}) \frac{\int ds \frac{\sigma_{p\gamma}(s)}{s - m_p^2}}{\int ds \frac{\sigma_{A\gamma}(s)}{s - m_A^2}} \left[ \left( \frac{s_{\text{GDR}} - m_A^2}{s_\Delta - m_p^2} \right) \left( \frac{\tilde{\varepsilon}_{p0}^\Delta}{\varepsilon_i^{\text{max}}} \right) \right]^{\alpha_\gamma - 1} \quad (30)$$

The importance of this relationship was highlighted in Ref. [37] (see also Eq. 6 of Ref. [57]). The survival condition is imposed by  $t'_{\text{dyn}} < t'_{\text{dis}}$ , which leads to

$$\tau_{A\gamma}(\varepsilon_i^{\text{max}}) \lesssim A, \quad (31)$$

which is analogous to Eq. (17). We get

$$\tau_{p\gamma 0} \lesssim A \frac{\int ds \frac{\sigma_{p\gamma}(s)}{s - m_p^2}}{\int ds \frac{\sigma_{A\gamma}(s)}{s - m_A^2}} \left[ \left( \frac{s_{\text{GDR}} - m_A^2}{s_\Delta - m_p^2} \right) \left( \frac{\tilde{\varepsilon}_{p0}^\Delta}{\varepsilon_i^{\text{max}}} \right) \right]^{\alpha_\gamma - 1}. \quad (32)$$

In particular, for  $\alpha_\gamma = 1.0$ , this leads to  $\tau_{p\gamma} \sim \tau_{p\gamma 0} \lesssim 0.4 (A/56)^{0.79}$ , which is equivalent to Eq. 10 of Ref. [57]. (Note that the value itself can be enhanced by the quasid neutron process, baryon resonances and photofragmentation.) We require this survival condition in addition to Eqs. (1), (15) and (16). It should be noted that this constraint is stronger for  $\alpha_\gamma > 1$ .

The aforementioned requirements of the sources are applied independently of the details of the UHECR composition. However, the constraints from the diffuse UHECR and neutrino fluxes depend on the composition. Even if UHECRs are dominated by nuclei, the lower-energy cosmic rays that are responsible for IceCube neutrinos may be proton dominated, in which the diffuse constraints remain unchanged from those obtained in the previous subsections. However, if the cosmic rays are dominated by heavy nuclei even at lower energies, the constraints are modified. We hereby consider such cases. The astrophysical neutrino flux from the UHECR nuclei can be approximately described using a treatment similar to the case of proton-dominated UHECRs, if the UHECR sources are effectively transparent to the photodisintegration process. The neutrino flux due to photomeson production via secondary nucleons and primary nuclei is given by

$$\begin{aligned} E_\nu^2 \frac{dJ_\nu}{dE_\nu} &\approx \frac{3}{8} [1 - (1 - \kappa_{p\gamma})^{\tau_{p\gamma}}] [1 - (1 - \kappa_{\text{dis}})^{\tau_{A\gamma}}] E_i^2 \frac{dJ_{\text{CR}}}{dE_i} \\ &+ \frac{3}{8} [1 - (1 - \kappa_{\text{mes}})^{\tau_{\text{mes}}}] (1 - \kappa_{\text{dis}})^{\tau_{A\gamma}} E_i^2 \frac{dJ_{\text{CR}}}{dE_i} \end{aligned} \quad (33)$$

Note that in the limit of  $\kappa_{p\gamma} \ll 1$  and  $\kappa_{\text{dis}} \ll 1$  keeping  $\kappa_{p\gamma} \tau_{p\gamma} < 1$  and  $\kappa_{A\gamma} \tau_{A\gamma} < 1$ , we have

$$\begin{aligned} E_\nu^2 \frac{dJ_\nu}{dE_\nu} &\approx \frac{3}{8} \kappa_{p\gamma} \tau_{p\gamma} [E_i/A] \kappa_{\text{dis}} \tau_{A\gamma} E_i^2 \frac{dJ_{\text{CR}}}{dE_i} \\ &+ \frac{3}{8} \kappa_{\text{mes}} \tau_{\text{mes}} [E_i] (1 - \kappa_{\text{dis}} \tau_{A\gamma}) E_i^2 \frac{dJ_{\text{CR}}}{dE_i}, \end{aligned} \quad (34)$$

which is similar to Eq. (11) of Ref. [57]. The first term of the right hand side represents the contribution from secondary nucleons while the second term is for the contribution from the photomeson production on nuclei.

With  $\tau_{\text{mes}}[E_i] \sim A \tau_{p\gamma} [E_i/A]$  (because of the approximation,  $\sigma_{\text{mes}}[E_i] \sim A \sigma_{p\gamma} [E_i/A]$ ) and  $\kappa_{\text{mes}}[E_i] \sim \kappa_{p\gamma} [E_i/A]/A$ , we approximately obtain [57]

$$E_\nu^2 \frac{dJ_\nu}{dE_\nu} \approx \frac{3}{8} \kappa_{p\gamma} \tau_{p\gamma} [E_i/A] E_i^2 \frac{dJ_{\text{CR}}}{dE_i} \quad (35)$$

We stress that this formula is derived assuming that all UHECRs are nuclei. Then, noting that  $E_i \approx AE_p$ , we

have

$$E_\nu^2 \frac{dJ_\nu}{dE_\nu} \approx \frac{3}{8} \kappa_{p\gamma} \tau_{p\gamma} [E_p] E_p^2 \frac{dJ_{\text{CR}}}{dE_p} A^{2-\alpha_{\text{CR}}}. \quad (36)$$

Finally, the results on such a nuclear case is obtained by introducing the following ‘‘correction’’ to the proton case considered before, which is

$$E_\nu^2 \frac{dJ_\nu}{dE_\nu} \approx E_\nu^2 \frac{dJ_\nu^{(p)}}{dE_\nu} A^{2-\alpha_{\text{CR}}}. \quad (37)$$

This is simply because a neutrino with  $E_\nu$  mainly originates from nuclei with  $E_A \sim 20AE_\nu$ . Thus, the diffuse constraints derived because the proton composition is regarded as conservative.

We ‘‘require’’ that the sources should be effectively transparent to the photodisintegration process, and the spectrum of escaping cosmic rays should be the same as that of the accelerated rays up to  $E_i^{\text{max}}$ . We assume that the flux of escaping UHECRs is the same as that of the accelerated UHECRs up to  $E_i^{\text{max}}$ . As previously discussed, the spectrum of escaping cosmic rays can be significantly different. This is usually expected in radiation-rich environments such as GRBs [37] and blazars [25]. However, diffuse environments such as galaxy clusters are also plausible examples [6]. In general, such a case requires detailed analyses but analytical formulas are adequate for this work.

Fig. 9 shows the resultant constraints (for  $\alpha_\gamma = 1.0$ ). In this case, we consider silicon ( $A = 28$ ) UHECRs as a benchmark. Both the acceleration and escape conditions are considered. The allowed region in the  $L'_\gamma - N_\Gamma$  plane is similar but wider than that of the proton-dominated case. The allowed region for  $\tau_{p\gamma 0}$  is smaller in the nuclei case because of the nucleus-survival condition – a photon field that facilitates the survival of nuclei is indicative of a low efficiency of photo-meson production. For the nucleus-survival condition, the constraints become even more stringent as indicated by the vertical line in the figure. This may suggest that fine-tuning is needed to build a viable model of UHECR nuclei sources. When the target photon spectrum is softer, the resultant parameter space is even smaller compared to the proton-dominated case.

## V. CANDIDATE SOURCES

In this section, we consider different source classes. The list of candidate sources for the unified photo-hadronic scenario is given in Table I.

### A. High-luminosity gamma-ray bursts

HL GRBs are among the most powerful gamma-ray transient sources, which are classically attributed to radiation from nonthermal electrons. They are also potential candidate sources of UHECRs because of their

high luminosity and large Lorentz factors [58–60] (see also Refs. [37, 61, 62] for applications to nuclei). With  $L_\gamma \sim 10^{51-53}$  erg s $^{-1}$  and  $\Gamma \sim 300$  [63], we have the comoving (isotropic-equivalent) luminosity,  $L'_\gamma \sim 10^{46-48}$  erg s $^{-1}$ . The magnetic energy density is assumed to be comparable to that of the radiation luminosity if the synchrotron peak is near the observed peak energy at  $\varepsilon_\gamma^b \approx \Gamma \hbar \gamma_b'^2 \frac{eB'}{m_e c} \sim 300$  keV. This implies  $B' \sim 10^3 - 10^5$  G for the electron Lorentz factor  $\gamma_b' \sim 10^3 - 10^4$ . This can be compatible with  $\xi_B \sim 0.01 - 100$ . UHECR acceleration is allowed based on the luminosity argument [37, 64]. The low-energy index of the target photon spectrum (below the peak energy near  $\varepsilon_\gamma^b \sim 1$  MeV) is relevant for UHECRs, typically  $\alpha_\gamma \sim 1$ , in which the photo-meson production optical depth is approximately energy independent (although multipion production enhances it by a factor of 3 [36]). The apparent rate density of HL GRBs and the duration are  $\rho \sim 1$  Gpc $^{-3}$  yr $^{-1}$  [65] and  $\Delta T \sim 30$  s, respectively. This gives  $n_0 \sim 10^{-15}$  Mpc $^{-3}$ . The constraint shown in Fig. 3 indicates that  $N_\Gamma \sim 10^{-9}$  Mpc $^{-3}$  (see also Figs. 2 and 5 for the cases with  $\Gamma \sim 100 - 1000$ ), which leads to  $\xi_{\text{CR}} \sim 10(\Gamma/300)^{-2}$ . This is consistent with the value required based on the GRB-UHECR hypothesis [37].

One of the advantages of HL GRB models is that the steepening of neutrino spectra above a few PeV energies can readily be explained (see Fig. 2). This is because the strong cooling of pions and muons suppresses the high-energy neutrino spectrum [11]. However, the photo-meson production optical depth required for the unification model is  $\tau_{p\gamma} \sim 0.1 - 0.6$ , which strongly constrains the HL GRB models. HL GRBs are so bright that stacking limits are very impactful, and the recent IceCube analysis gives the stringent limit,  $\tau_{p\gamma} \lesssim 0.05$  [66–68] and challenges the GRB-UHECR models [69, 70]. The null detection of cosmogenic neutrinos by IceCube also substantially constrained the possibility that the HL GRBs are a significant population of UHECR sources [46]. Thus, although the allowed parameter space may be compatible with the GRB models, we conclude that HL GRBs are unlikely to provide a unified explanation for UHECRs and PeV neutrinos.

### B. Low-luminosity gamma-ray bursts and transrelativistic supernovae

Engine-driven supernovae with a Lorentz factor of  $\Gamma\beta \gtrsim 0.1 - 1$  have been proposed as the main sources of UHECRs [13–15, 37, 71]. Note that this category includes LL GRBs like GRN 060218 [72], peculiar hypernovae like SN 2009bb [73], and fast-rising blue optical transients such as AT2018cow [73, 74]. If the jet scenario is assumed, with  $L_\gamma \sim 10^{46-48}$  erg s $^{-1}$  and  $\Gamma \sim 3$ , we have  $L'_\gamma \sim 10^{45-47}$  erg s $^{-1}$ . The luminosity requirement can be satisfied only for optimistic parameters, e.g.,  $L_\gamma \sim 10^{48}$  erg s $^{-1}$ , but it can be more readily fulfilled if UHECRs are heavy nuclei, as opposed

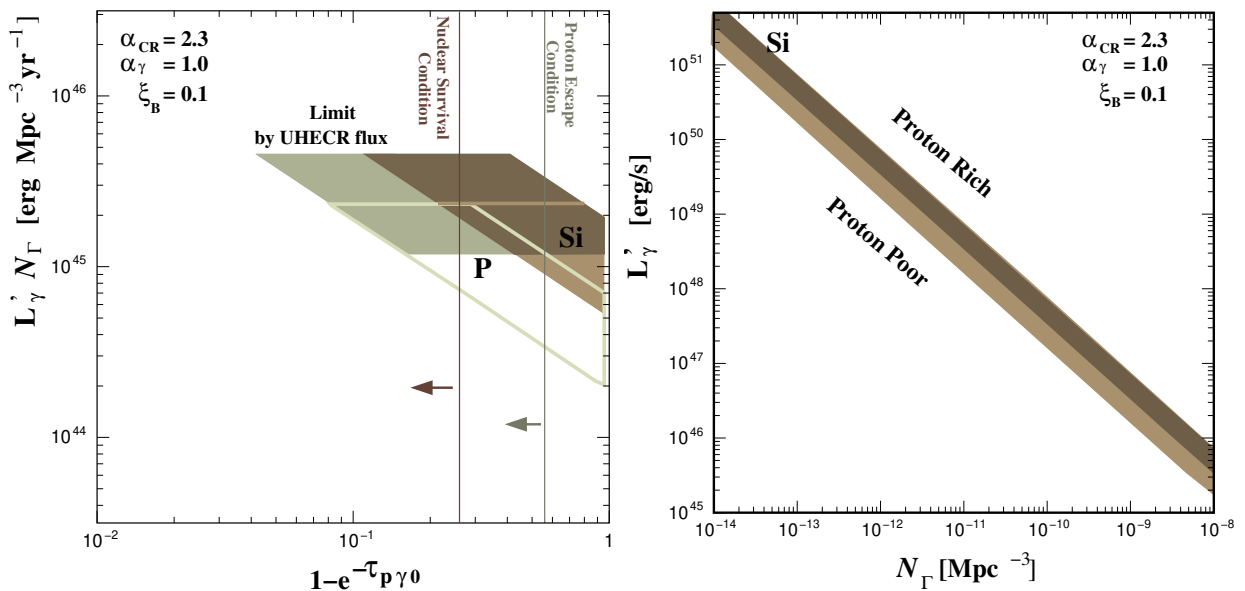


FIG. 9. Same as Fig. 3 but show the case of primary silicon nuclei. In the left plot, the constraints for the silicon case is overlaid with the proton case for comparison. The horizontal belt represented by the darker shade shows the systematics of UHECR energetics that originate due to the uncertainties associated with the mass composition and galactic to extra-galactic transition of UHECRs [38]. The darker shaded region in the right panel represents the allowed space when the nuclear-survival condition is required.

TABLE I. Characteristic parameters of the candidate sources of UHECRs and high-energy neutrinos.

	HL GRB	LL GRB	Newborn magnetar	Jetted TDEs	Blazar Flares	Jetted AGN
$L_\gamma$ [erg s $^{-1}$ ]	$10^{51-53}$	$10^{46-48}$	$10^{42-44}$	$10^{45-48}$	$10^{45-48}$	$10^{43-48}$
$\Gamma$	100 – 1000	2 – 30	?	3 – 100	3 – 100	3 – 100
$\rho$ [Gpc $^{-3}$ yr $^{-1}$ ]	0.1 – 1	100 – 1000	1000 – 10000	0.01 – 0.1	100 – 1000	—
$\Delta T$ [s]	10 – 1000	100 – 10000	$10^{2-5}$	$10^{5-7}$	$10^{5-7}$	—

to considering protons [37, 75]. The rate density and duration are  $\rho \sim 100 - 1000 \text{ Gpc}^{-3} \text{ yr}^{-1}$  and  $\Delta T \sim 3000 \text{ s}$ , respectively [72, 76, 77], which should be compared to  $N_\Gamma \sim 10^{-9} \text{ Mpc}^{-3}$  from Fig. 3. The effective number density is  $n_0 \sim 10^{-11} - 10^{-10} \text{ Mpc}^{-3}$  and the condition can be satisfied if  $\zeta_{\text{CR}} \sim (1 - 10)(\Gamma/3)^{-2}$ .

The peak energy of GRB 060218 and GRB 100316D is  $\varepsilon_\gamma^b \sim 1 - 10 \text{ keV}$  [76]. The magnetic field strength is not well understood, but  $\xi_B \sim 0.1 - 10$  is expected in the case of the synchrotron. For  $\alpha_\gamma \sim 1$ , the optical depth required for photo-meson production is estimated to be  $\tau_{p\gamma} \sim 0.01 - 1$  [13]. It should be noted that such a hard photon spectrum is necessary to maintain consistency with optical observations [13, 75]. Thus, we conclude that LL GRBs could be viable sources of high-energy neutrinos and UHECRs if the luminosity is higher and/or if cosmic rays are nuclei, which is consistent with previous works [37, 78].

However, it should be considered that the mechanism of prompt emission from LL GRBs is still under debate, and another (more promising) possibility is the

shock breakout scenario [76], in which gamma rays are attributed to shock breakout from a mildly relativistic outflow (that may be driven by a jet). In this scenario, UHECRs are unlikely to be generated during the prompt phase [79]. Although IceCube neutrinos are explained by choked jets or transrelativistic shocks in a dense wind [80], UHECRs acceleration is attributed to a later transrelativistic component that is decelerated over the time scale of weeks or months [31].

### C. Newborn magnetars

Some of the supernovae are more powerful than ordinary supernovae, and are referred to as hypernovae. Their ejecta are either nonrelativistic or transrelativistic (i.e., the Lorentz factor is  $\Gamma\beta \gtrsim 0.1 - 1$ ), which may be driven by some central engine with possible candidates that include a newborn magnetar (e.g., [81]), a fallback disk around a black hole (e.g., [82]), and collisions with dense circumstellar material (e.g., [83]).

We discuss the newborn magnetar scenario that has been widely discussed in the recent literature. The spin-down luminosity is  $L_{\text{sd}} \sim 3 \times 10^{49} \text{ erg s}^{-1}$  for a millisecond rotating magnetar with a dipole magnetic field of  $\sim 10^{15} \text{ G}$ . Efficient ion acceleration could occur inside a relativistic wind [84], in which the square of the additional factor  $\theta_{\text{mag}} = R_s 2\pi / (cP) \sim 0.2(P/1 \text{ ms})$  should be included as part of the luminosity requirement. Although the UHECR acceleration is possible in this magnetar scenario [84], the photons associated with the dissipation of Poynting dominated winds should be thermalized inside the supernova ejecta. Therefore, our power-law assumption for the photon spectrum may not hold. Furthermore, the model typically predicts neutrino emission in the EeV range rather than in the PeV range [16, 17]. As such, it is difficult to explain the situation of IceCube neutrinos in the PeV range using the fiducial model. Thus, this model is not discussed in further detail. Finally, we also note that the IceCube EHE neutrino limit in the EeV range has already started to strongly constrain the magnetar scenario [46].

#### D. Tidal disruption events

TDEs originate from the disruption of a main-sequence star or white dwarf by a supermassive black hole or an intermediate-mass black hole, respectively. Some of the TDEs have powerful jets, and the X-ray luminosity of Sw J1644+57 was  $L_\gamma \sim 10^{47-48} \text{ erg s}^{-1}$  [85]. For  $\Gamma \sim 10$ , we have  $L'_\gamma \sim 10^{46-47} \text{ erg s}^{-1}$ . Thus the luminosity requirement can be satisfied [86]. The apparent rate density and duration are  $\rho \sim 0.01 - 0.1 \text{ Gpc}^{-3} \text{ yr}^{-1}$  and  $\Delta T \sim 3 \times 10^6 \text{ s}$ , respectively. Thus the effective number density becomes  $n_0 \sim 10^{-12} - 10^{-11} \text{ Mpc}^{-3}$ . In comparison to  $N_\Gamma \sim 10^{-9} \text{ Mpc}^{-3}$  from Fig. 3, the condition for the unification of UHECRs and PeV neutrinos can be satisfied if  $\xi_{\text{CR}} \sim (1 - 10)(\Gamma/10)^{-2}$ .

The most common explanation for x rays from Sw J1644+57 is non-thermal synchrotron emission, and the peak energy is  $\epsilon_\gamma^b \approx \Gamma \hbar \gamma_b^2 \frac{eB'}{m_e c} \sim 100 \text{ keV}$  [85], which implies that  $B' \sim 10^2 - 10^4 \text{ G}$  for the electron Lorentz factor  $\gamma_b' \sim 10^4 - 10^5$ . These can be compatible with  $\xi_B \sim 0.01 - 100$ . However, provided that we consider UHECR production inside jets of TDEs such as Sw J1644+57, strong radiation fields lead to  $\tau_{p\gamma 0} \gg 1$  [87], which makes it difficult to find parameters that satisfy the constraints in Fig. 3. The problem is worse if we require the nucleus-survival condition because nuclei are disintegrated in the presence of such intense radiation fields [20, 31]. It has been suggested that hypothetical low-luminosity or low-state TDEs with  $L_\gamma \sim 10^{45-46} \text{ erg s}^{-1}$  are necessary for nuclei to survive, based on which the UHECR flux could be explained [20, 31]. Alternatively, cosmic-ray acceleration at external shocks formed by jets or winds is also possible [31, 88], although efficient PeV neutrino production is not expected in these scenarios.

Our results imply that low-luminosity TDEs that al-

low  $\tau_{p\gamma 0} \lesssim 1$  can satisfy the required conditions for the unification model, but nuclei rather than protons are required to obtain the highest energies. Correspondingly, the required cosmic-ray loading factors would be larger. With  $N_\Gamma \sim 3 \times 10^{-8} \text{ Mpc}^{-3}$ , we obtain  $\xi_{\text{CR}} \sim (30 - 300)(\Gamma/10)^{-2}$  (see also [20, 21, 31]). However, it is unlikely that TDEs are the common sources of IceCube neutrinos and UHECRs for several different reasons. It has been shown that it is difficult for TDEs to be the dominant population in the diffuse IceCube flux. TDEs are so rare that the limits due to the absence of neutrino multiple sources in the IceCube data are stringent [87]. Furthermore, there is no evidence of positive neutrino signals from Sw J1644+57 and other TDEs [89]. Recently, it has been claimed that IceCube-191001A could coincide with TDE AT2019dsg [90, 91], but the physical association is still questionable [92] although AT2019dsg is thought to be a rare, luminous class of TDEs.

#### E. Blazar flares and jetted active galactic nuclei

Some active galactic nuclei (AGNs) have relativistic jets, and such jetted AGNs are considered as promising candidate sources of UHECRs and high-energy neutrinos. Recent studies have argued that steady emission of jetted AGNs is unlikely to be the source of UHECRs, especially if the UHECR composition is dominated by protons. Fanaroff-Riley II (FR II) galaxies and flat-spectrum radio quasars (FSRQs) can satisfy the Hillas condition, Eq. (1), but they are too rare in the local universe within 100 Mpc [93, 94]. This difficulty can be overcome if the UHECRs are accelerated during the active/flaring phase, for which the luminosity requirement is satisfied [95, 96].

A typical AGN luminosity is  $L_j \sim 10^{44} \text{ erg/s}$ , and the isotropic-equivalent luminosity can be enhanced by  $2/\theta_j^2$ . The importance of flaring emission has been strengthened based on the recent discovery of IceCube-170922A that coincided with the flaring blazar TXS 0506+056 [97], although this blazar was not favored as an UHECR accelerator [98].

The magnetic field strength can be estimated from the Compton dominance parameter. The leptonic modeling of FSRQs often suggests  $U'_\gamma \gtrsim U'_B$ , and  $B' \sim 0.1 - 10 \text{ G}$  is typically expected for FSRQs [26, 99], which corresponds to  $\xi_B \lesssim 0.01 - 1$ . However, the survival of heavy nuclei is typically difficult in FSRQs, whereas low-luminosity BL Lacs allow nuclei to survive, although the photo-meson production optical depth is expected to be low [25, 26]. In the leptohadronic scenario (which includes the proton synchrotron scenario), higher magnetic fields,  $B' \sim 10 - 100 \text{ G}$ , may be required [100, 101] but such highly magnetized environments may be highly demanding for jet physics and may be contradictory to the nucleus-survival condition (see Eq. 16).

Furthermore, UHECR emission from Fanaroff-Riley (II) galaxies/FSRQs is not favored given that strongly evolved UHECR sources are not favored by the IceCube

EHE limit [46] as well as constraints from the absence of small-scale anisotropies. Thus, it is unlikely that the jetted AGNs are responsible for the observed UHECRs if they are dominated by protons.

Ref. [26] proposed the scenario whereby EeV neutrinos are dominated by FSRQs, whereas UHECRs are dominated by BL Lac objects (see also Ref. [102]). However, the spectrum of neutrinos is typically expected in the EeV range, so the IceCube neutrino flux is not accounted for simultaneously. The reason is as follows. The photo-meson production efficiency cannot decrease with the increase of energy. Even for FSRQs, where external radiation fields are usually dominant as target photons,  $\tau_{p\gamma}$  has an energy-independent behavior beyond the pion production threshold due to the multipion production [26]. For BL Lacs, radiation from inner jets is typically more important, and the rectangular approximation around the  $\Delta$  resonance can be justified. Then, from Eq. (12), 1 PeV neutrinos typically originate from photons with  $\sim 0.8 (\Gamma/10)^2$  keV. Except for extremely high synchrotron peaked BL Lacs, the spectral index in the X-ray range is around  $\alpha_\gamma \sim 1.5-3$ , so the number of target photons is larger at lower energies. As a result, for both BL Lacs and FSRQs, the spectrum of neutrinos is predicted to be hard in the PeV range since  $\Phi_\nu \propto E_\nu^{-(\alpha_{\text{CR}}+1-\alpha_\gamma)}$  as shown in Eq. (A3) (e.g., [22, 23, 26, 103–105] for model-dependent numerical calculations). This contradicts the diffuse limits [46] if the cosmic-ray spectrum is extended to ultrahigh energies with a simple power law [98, 106].

For example, the conclusion determined based on the model-dependent calculations for BL Lacs (that may allow the survival of nuclei) can be interpreted using Figs. 5 and 6 considering our generic, model-independent constraints. To compensate for a soft target spectrum with  $\alpha_\gamma > 1$ , a softer UHECR spectrum is required to supply the substantial amount of PeV energy cosmic rays as discussed in Section IV B. For  $\alpha_\gamma = 1.5$  and  $\alpha_{\text{CR}} = 2.3$ , we see that the model violates the IceCube EHE limit unless  $\Gamma$  is very large. Given that  $\Gamma \lesssim 10-100$  is expected for blazars, the cosmic-ray spectral index  $\alpha_{\text{CR}}$  must be larger than 2.3 (see Fig. 7). Such cases are not excluded but the required energetics is more demanding.

## VI. SUMMARY AND DISCUSSION

We explored the viability of the unification model for UHECRs and IceCube neutrinos considering photo-hadronic scenarios, in which neutrinos are produced by the interactions between high-energy ions and low-energy photons. The results are summarized as follows.

- By requiring necessary conditions for UHECR sources, including those for acceleration (i.e., the Hillas condition) and survival, we obtained constraints on the photo-meson production optical depth in the UHECR sources. We further combined these source constraints with observational

constraints imposed by the neutrino data from IceCube as well as the UHECR data from Auger.

- We found the viable parameter space required to explain the diffuse high-energy neutrino flux above 100 TeV energies and the UHECR flux above 10 EeV, simultaneously. The allowed regions of  $\tau_{p\gamma 0}$  and  $Q_{\text{CR}} = N_\Gamma L'_\gamma$  depend on  $\alpha_{\text{CR}}$ ,  $\alpha_\gamma$ , and  $\Gamma$ . For  $\alpha_{\text{CR}} = 2.2$  and  $\alpha_\gamma = 1.0$ , we found  $0.1 \lesssim \tau_{p\gamma} \lesssim 0.6$  regardless of  $\Gamma$ , which can be shifted to lower values for larger  $\alpha_{\text{CR}}$  and/or smaller  $\alpha_\gamma$ . We also suggested the cooling break scenario, wherein the observed softness of the neutrino spectrum in the multi-PeV range can be explained by the suppression due to the cooling of mesons and muons.
- The Auger data on the UHECR composition have suggested that the UHECRs are likely to be dominated by intermediate to heavy nuclei above the ankle. The existence of nuclei imposes an additional condition on their survival due to the photodisintegration process. We showed that the allowed parameter space is narrower than the case of only protons. This is mainly because the nucleus-survival condition results in tighter upper limits on the photo-meson production optical depth, therefore, it is more difficult for hard CR spectra and/or soft photon spectra to match the IceCube data. This situation is even more prominent if the observed neutrinos originate from nuclei rather than protons because the neutrino intensity is suppressed by  $A^{\alpha_{\text{cr}}-2}$  compared to the proton case (see Eq. 37). For example, with  $\alpha_{\text{CR}} \sim 2.3$  and  $\alpha_\gamma \sim 1.0$  in the silicon composition case, we obtained  $\tau_{p\gamma} \sim 0.1 \sim 0.2$ , which is consistent with the nucleus-survival bound derived by Ref. [57]. The allowed parameter space is almost unique for  $\alpha_{\text{CR}} \sim 2.3$  and  $\alpha_\gamma \sim 1.0$ , which can be used as one of the critical tests for the unification model with cosmic-ray accelerators.
- In general, we derived more conservative constraints that are imposed by matching the IceCube data without overshooting the Auger data. The allowed parameter space is extended, especially for steeper cosmic-ray spectra, because larger values of the photo-meson production optical depths are possible. It should be noted that in this case, the proton component is subdominant so UHECRs should be dominated by nuclei for a viable unification model.
- Based on the conditions derived in this work, we examined different classes of astrophysical sources that could be viable as the sources of  $p\gamma$  neutrinos for the unification model. We found that among the known source classes, LL GRBs and jetted TDEs can be viable, but the results of recent studies suggest that the latter source class is likely to be subdominant as the origin of the diffuse neutrino flux. However, we stress that our constraints are generic,

and we do not exclude the possibility of other unknown source candidates.

The grand-unification model that accounts for the gamma-ray data has been discussed, especially for the hadronuclear scenario [6, 8]. We did not explicitly calculate the extragalactic gamma-ray background that is expected in the photohadronic scenario for the unification model, because it is highly model-dependent. In our case, gamma rays produced inside the sources are likely to be cascaded inside the sources. There is a correspondence between the optical depth to the  $\gamma\gamma \rightarrow e^+e^-$  process and the  $p\gamma$  optical depth  $\tau_{p\gamma}$ . Lower limits of the  $p\gamma$  optical depth [33] suggest that it is more natural for the sources to be optically thick to GeV-TeV gamma rays [35]. However, there is an unavoidable contribution of cosmogenic gamma rays induced by UHECRs, which can give rise to a significant contribution to the extragalactic gamma-ray background, especially in GRB and AGN models that have strong redshift evolution.

We note that the main purpose of this work is to obtain necessary constraints for the unification model with photohadronic neutrinos. As shown in this work, even the necessary conditions impose strict constraints, and

can allow us to determine some implications for various types of possible candidate sources. We expect that the quantitative fitting of the data is possible but detailed analyses are left for future work. In this case, we note that there is a large uncertainty that originates from the UHECR escape mechanism. In the cosmic-ray accelerator models that are considered in this work, the parameter  $\alpha_{\text{CR}}$  should be regarded as the spectral index of the accelerated cosmic rays, which can be significantly different from that of the escaping UHECRs, especially for transient sources [15, 19, 31]. As a result, the spectrum of UHECRs injected into intergalactic space can be harder [107]

## ACKNOWLEDGMENTS

The authors are grateful to Markus Ahlers and Francis Halzen for their valuable comments on the manuscript. This work by S.Y. is supported by JSPS KAKENHI Grant No. 18H05206 and Institute for Global Prominent Research (IGPR) of Chiba University; The work of K.M. is supported by the Alfred P. Sloan Foundation, NSF Grant No. AST-1908689, and JSPS KAKENHI No. 20H01901.

## Appendix A: Analytical Formulas for calculating neutrino flux

The energy flux integral, Eq. (25), is transformed to the neutrino intensity bases as

$$\Phi_\nu(E_\nu) = \frac{cn_0}{4\pi} \int_0^{z_{\text{max}}} dz \psi(z)(1+z) \left| \frac{dt}{dz} \right| \frac{d\dot{N}_\nu}{d\varepsilon_\nu}(\varepsilon_\nu, z), \quad (\text{A1})$$

The energy distribution of neutrinos generated from an interaction that appeared in Eq. (21) is given by

$$Y(\varepsilon_\nu; \varepsilon_i, s) = \frac{1}{\sigma_{p\gamma}} \int d\varepsilon_\pi \frac{d\sigma_{p\gamma \rightarrow \pi}}{d\varepsilon_\pi}(\varepsilon_\pi; \varepsilon_i, s) \frac{dn_{\pi \rightarrow \nu}}{d\varepsilon_\nu}(\varepsilon_\nu; \varepsilon_\pi), \quad (\text{A2})$$

where  $\sigma_{p\gamma \rightarrow \pi}$  is the inclusive cross-section of  $p\gamma$  collisions with pion multiplicity taken into account and the last term is the neutrino spectrum from pion decay.

Following the analytical formulation in Ref. [33], we finally obtain

$$\frac{dJ_\nu}{dE_\nu}(E_\nu) \simeq \frac{n_0 \tau_{p\gamma 0}}{(\alpha_{\text{CR}} + 1 - \alpha_\gamma)^2} \frac{K_{\text{CR}}}{\varepsilon_{i0}} \frac{c}{H_0} \frac{s_\Delta}{\sqrt{(s_\Delta + m_\pi^2 - m_p^2)^2 - 4s_\Delta m_\pi^2}} \frac{3}{1 - r_\pi} \left( \frac{E_\nu}{\varepsilon_{i0}(x_{\text{R}}^+(1 - r_\pi))} \right)^{-(\alpha_{\text{CR}} + 1 - \alpha_\gamma)} \zeta. \quad (\text{A3})$$

The factor of three corresponds to the number of neutrinos produced from the  $\pi$  meson and  $\mu$  lepton decay chain. The factor  $\zeta$  is the term that accounts for the redshift dependence and is given by,

$$\zeta = \left[ I_1(z_{\text{down}}, z_\mu) + \frac{1}{3} I_1(z_\mu, z_\pi) + \frac{2}{3} \left( \frac{E_\nu}{\Gamma \varepsilon_\mu^{\text{syn}}} \right)^{-2} I_2(z_\mu, z_{\text{max}}) + \frac{1}{3} \left( \frac{E_\nu}{\Gamma \varepsilon_\pi^{\text{syn}}} \right)^{-2} I_2(z_\pi, z_{\text{max}}) \right] \quad (\text{A4})$$

$$I_1(z_1, z_2) = \frac{2}{2(m - \alpha_{\text{CR}} + \alpha_\gamma) - 3} \Omega_{\text{M}}^{-\frac{m - \alpha_{\text{CR}} + \alpha_\gamma}{3}} \left[ \left\{ \Omega_{\text{M}}(1 + z_2)^3 + \Omega_\Lambda \right\}^{\frac{m - \alpha_{\text{CR}} + \alpha_\gamma}{3} - \frac{1}{2}} - \left\{ \Omega_{\text{M}}(1 + z_1)^3 + \Omega_\Lambda \right\}^{\frac{m - \alpha_{\text{CR}} + \alpha_\gamma}{3} - \frac{1}{2}} \right],$$

$$I_2(z_1, z_2) = \frac{2}{2(m - \alpha_{\text{CR}} + \alpha_\gamma) - 7} \Omega_{\text{M}}^{-\frac{m - \alpha_{\text{CR}} + \alpha_\gamma - 2}{3}} \left[ \left\{ \Omega_{\text{M}}(1 + z_2)^3 + \Omega_\Lambda \right\}^{\frac{m - \alpha_{\text{CR}} + \alpha_\gamma}{3} - \frac{7}{6}} - \left\{ \Omega_{\text{M}}(1 + z_1)^3 + \Omega_\Lambda \right\}^{\frac{m - \alpha_{\text{CR}} + \alpha_\gamma}{3} - \frac{7}{6}} \right].$$

The redshift bound  $z_{\text{down}}$  and  $z_{\pi,\mu}$  are the bounds of the redshift on the UHECR sources that contribute to the neutrino flux, which are constrained by the  $p\gamma$  interaction threshold and the synchrotron cooling of pion (muon), respectively. They are described as

$$1 + z_{\text{down}} = \begin{cases} 1 + z_{\text{max}} & \left( E_\nu < \frac{s_\Delta - m_p^2}{4(1+z_{\text{max}})} \frac{\Gamma}{\varepsilon'_\gamma \text{max}} x_{\text{R}}^+(1 - r_\pi) \right) \\ \frac{s_\Delta - m_p^2}{4} \frac{\Gamma}{\varepsilon'_\gamma \text{max}} \frac{x_{\text{R}}^+(1 - r_\pi)}{E_\nu} & \left( \frac{s_\Delta - m_p^2}{4(1+z_{\text{max}})} \frac{\Gamma}{\varepsilon'_\gamma \text{max}} x_{\text{R}}^+(1 - r_\pi) \leq E_\nu \leq \frac{s_\Delta - m_p^2}{4} \frac{\Gamma}{\varepsilon'_\gamma \text{max}} x_{\text{R}}^+(1 - r_\pi) \right) \\ 1 & \left( \frac{s_\Delta - m_p^2}{4} \frac{\Gamma}{\varepsilon'_\gamma \text{max}} x_{\text{R}}^+(1 - r_\pi) < E_\nu \right), \end{cases} \quad (\text{A5})$$

and

$$1 + z_{\pi,\mu} = \begin{cases} 1 + z_{\text{max}} & \left( E_\nu < \frac{\Gamma \varepsilon'_{\nu,\pi,\mu} \text{syn}}{1 + z_{\text{max}}} \right) \\ \frac{\Gamma \varepsilon'_{\nu,\pi,\mu} \text{syn}}{E_\nu} & \left( \frac{\Gamma \varepsilon'_{\nu,\pi,\mu} \text{syn}}{1 + z_{\text{max}}} \leq E_\nu < \Gamma \varepsilon'_{\nu,\pi,\mu} \text{syn} \right) \\ 1 & \left( \Gamma \varepsilon'_{\nu,\pi,\mu} \text{syn} \leq E_\nu \right). \end{cases} \quad (\text{A6})$$

The third (fourth) term in the bracket in Eq. A4 represents the spectrum of neutrinos from synchrotron-cooled muons (pions). It should be noted that  $z_{\text{down}} \leq z_\mu < z_\pi$  as the synchrotron loss determines the maximal energy of neutrinos in the presented model and  $\varepsilon'_{\nu,\mu} \text{syn} < \varepsilon'_{\nu,\pi} \text{syn}$ .  $\varepsilon'_{\nu,\pi/\mu} \text{syn} = \Gamma \varepsilon'_{\nu,\pi/\mu}$  is given by Eq. (23).

$x_{\text{R}}^+$  in Eqs. A3 and A5 is the maximal bound of the relative energy of emitted pion normalized by the parent cosmic-ray energy. They are represented by a kinematic relation (see Eq.(6) of Ref. [48]),

$$x_{\text{R}}^+ = \frac{(s_\Delta + m_\pi^2 - m_p^2) + \sqrt{(s_\Delta + m_\pi^2 - m_p^2)^2 - 4s_\Delta m_\pi^2}}{2s_\Delta}. \quad (\text{A7})$$

## Appendix B: Analytical formulas for estimating extragalactic UHECR intensity

The spectrum of UHECRs injected from sources is assumed to follow a power-law form, that is

$$\frac{d\dot{N}_{\text{CR}}}{d\varepsilon_i} = \frac{K_{\text{CR}}}{\varepsilon_{i0}} \left( \frac{\varepsilon_i}{\varepsilon_{i0}} \right)^{-\alpha_{\text{CR}}} e^{-\varepsilon_i/\varepsilon_i^{\text{max}}}. \quad (\text{B1})$$

UHECRs propagate in extragalactic space and interact with CMBs via the Bethe-Heitler (BH) process  $\gamma_{\text{CMB}} p \rightarrow pe^+e^-$  and the photopion production. In the present study, we approximate that the energy attenuation length of UHECR is constant with energies between  $E_{\text{BH}}$  and  $E_{\text{GZK}}$  governed by the BH process, written as  $\lambda_{\text{BH}}$ , and becomes another constant value  $\lambda_{\text{GZK}}$  at energies above  $E_{\text{GZK}}$  where the photopion production dominates the UHECR energy loss processes. This approximation reasonably describes the UHECR energy loss profile for the calculation of the resultant UHECR intensity on the Earth [108], although a more accurate estimation with a precision better than a factor of two requires dedicated numerical simulations. We set  $E_{\text{GZK}} = 6 \times 10^{10}$  GeV and  $E_{\text{BH}} = 2 \times 10^9$  GeV, respectively.

The behaviors of UHECR propagation can then be described by classifying their energies into five ranges for an UHECR source with a redshift of  $z_s$ , (A)  $\varepsilon_i < E_{\text{BH}}/(1 + z_s)$ , (B)  $E_{\text{BH}}/(1 + z_s) \leq \varepsilon_i, E_i < E_{\text{BH}}$ , (C)  $E_{\text{BH}} < E_i, \varepsilon_i \leq E_{\text{GZK}}/(1 + z_s)$ , (D)  $E_{\text{GZK}}/(1 + z_s) \leq \varepsilon_i, E_i < E_{\text{GZK}}$ , and (E)  $E_{\text{GZK}} \leq E_i$ .

### 1. $\varepsilon_i < E_{\text{BH}}/(1 + z_s)$ - The region of redshift loss only

When the UHECR energy for a source of redshift  $z_s$  is below the BH energy threshold  $\varepsilon_{\text{BH}} = E_{\text{BH}}/(1 + z_s)$ , only redshift energy loss occurs during the propagation. Given that  $E_i = \varepsilon_i/(1 + z_s)$ , this condition is equal to  $1 + z_s < \sqrt{E_{\text{BH}}/E_i}$ . The UHECR spectrum from this source is given by

$$\frac{d\dot{N}_{\text{CR}}}{dE_i} = \frac{K_{\text{CR}}}{\varepsilon_{i0}} (1 + z_s)^{-(\alpha_{\text{CR}} - 1)} \left( \frac{E_i}{\varepsilon_{i0}} \right)^{-\alpha_{\text{CR}}}. \quad (\text{B2})$$



Here  $E_i = \varepsilon_i/(1+z_s)$  is the observed UHECR energy.

The UHECR intensity is given by

$$\frac{dJ_{\text{CR}}}{dE_i} = \frac{n_0 c}{H_0} \int_{z_{\text{LB}}}^{z_{\text{UB}}} dz_s \frac{\psi(z_s)}{(1+z_s)\sqrt{\Omega_M(1+z_s)^3 + \Omega_\Lambda}} \frac{d\dot{N}_{\text{CR}}}{dE_i}, \quad (\text{B3})$$

where  $n_0$  is the comoving UHECR source number density in the local universe and  $\psi(z_s)$  is the cosmological evolution factor of UHECR sources and parameterized as  $(1+z_s)^m$  up to  $z_s = z_{\text{max}}$ .  $z_{\text{UB}}$  and  $z_{\text{LB}}$  are the lower and maximal bound of the source redshift distribution  $z_s$ , respectively. Since  $1+z_s < \sqrt{E_{\text{BH}}/E_i}$ , and UHECR sources are distributed between  $z_s = 0$  and  $z_s = z_{\text{max}}$ ,  $z_{\text{UB}}$  in the integral of Eq. B3 that is described by  $z_{\text{BH}}$ , which is a function of the UHECR energy on the Earth,  $E_i$ , and given by

$$1+z_{\text{BH}} = \begin{cases} 1+z_{\text{max}} & \left(E_i < \frac{E_{\text{BH}}}{(1+z_{\text{max}})^2}\right) \\ \sqrt{\frac{E_{\text{BH}}}{E_i}} & \left(\frac{E_{\text{BH}}}{(1+z_{\text{max}})^2} \leq E_i < E_{\text{BH}}\right) \\ 1 & (E_{\text{BH}} \leq E_i). \end{cases} \quad (\text{B4})$$

Obviously  $z_{\text{LB}} = 0$ .

Putting Eq. B2 into Eq. B3, we get

$$\frac{dJ_{\text{CR}}}{dE_i} \simeq n_0 \frac{K_{\text{CR}}}{\varepsilon_{i0}} \frac{c}{H_0} \left(\frac{E_i}{\varepsilon_{i0}}\right)^{-\alpha_{\text{CR}}} \frac{1}{2(m-\alpha_{\text{CR}})-1} \Omega_M^{-\frac{m-\alpha_{\text{CR}}+1}{3}} \left[ \left\{ \Omega_M(1+z_{\text{BH}})^3 + \Omega_\Lambda \right\}^{\frac{m-\alpha_{\text{CR}}}{3} - \frac{1}{6}} - 1 \right] \quad (\text{B5})$$

In this case, we use the approximated expression for the integral of the source redshift described in the appendix of Ref. [33].

## 2. $E_{\text{BH}}/(1+z_s) \leq \varepsilon_i, E_i < E_{\text{BH}}$ - The region of partial BH process and redshift loss

In this energy range, UHECR proton is subject to the redshift loss and the BH process during its propagation until its energy reaches the threshold energy of the BH process. Let us denote the redshift when the proton energy is equal to the BH threshold energy as  $z = \bar{z}_{\text{BH}}$ . In propagating from  $z = \bar{z}_{\text{BH}}$  to  $z = 0$ , only the redshift dilution reduces its energy. In this case, the UHECR proton energy on the Earth is related to  $E_{\text{BH}}$  by  $E_i = E_{\text{BH}}/(1+\bar{z}_{\text{BH}})^2$ . Hence  $\bar{z}_{\text{BH}}$  is effectively represented by Eq. B4. The UHECR proton energy at source  $\varepsilon_i$  is related to  $E_{\text{BH}}$  as

$$\varepsilon_i = E_{\text{BH}} \frac{1+z_s}{(1+z_{\text{BH}})^2} e^{\frac{c}{H_0 \lambda_{\text{BH}}}} \frac{2}{3\Omega_M} \left\{ \sqrt{\Omega_M(1+z_s)^3 + \Omega_\Lambda} - \sqrt{\Omega_M(1+z_{\text{BH}})^3 + \Omega_\Lambda} \right\} \quad (\text{B6})$$

The UHECR spectrum from a source is given by

$$\begin{aligned} \frac{d\dot{N}_{\text{CR}}}{dE_i} &= \int d\varepsilon_i \frac{d\dot{N}_{\text{CR}}}{d\varepsilon_i} \delta\left(E_i - \frac{E_{\text{BH}}}{(1+z_{\text{BH}})^2}\right) \\ &= \frac{c}{2H_0 \lambda_{\text{BH}}} \frac{K_{\text{CR}}}{\varepsilon_{i0}} (1+z_s)^{-(\alpha_{\text{CR}}-1)} \left(\frac{E_{\text{BH}}}{\varepsilon_{i0}}\right)^{-\alpha_{\text{CR}}} \frac{(1+z_{\text{BH}})^{2\alpha_{\text{CR}}+3}}{\sqrt{\Omega_M(1+z_{\text{BH}})^3 + \Omega_\Lambda}} \\ &\quad \times e^{-(\alpha_{\text{CR}}-1)\frac{c}{H_0 \lambda_{\text{BH}}}} \frac{2}{3\Omega_M} \left\{ \sqrt{\Omega_M(1+z_s)^3 + \Omega_\Lambda} - \sqrt{\Omega_M(1+z_{\text{BH}})^3 + \Omega_\Lambda} \right\}. \end{aligned} \quad (\text{B7})$$

Given that  $z_s \geq z_{\text{BH}}$  in this category of  $E_i$  range, the resultant intensity of the UHECRs emitted from all sources in space is then calculated using Eq. B3 with  $z_{\text{LB}} = z_{\text{BH}}$  and  $z_{\text{UB}} = z_{\text{max}}$ . We get

$$\begin{aligned} \frac{dJ_{\text{CR}}}{dE_i} &\simeq n_0 \frac{K_{\text{CR}}}{\varepsilon_{i0}} \frac{c}{H_0} \left(\frac{E_{\text{BH}}}{\varepsilon_{i0}}\right)^{-\alpha_{\text{CR}}} \frac{1}{2(\alpha_{\text{CR}}-1)} \frac{(1+z_{\text{BH}})^{2\alpha_{\text{CR}}+3}}{\sqrt{\Omega_M(1+z_{\text{BH}})^3 + \Omega_\Lambda}} \times \\ &\quad \left[ (1+z_{\text{BH}})^{m-\alpha_{\text{CR}}-2} - (1+z_{\text{max}})^{m-\alpha_{\text{CR}}-2} e^{-(\alpha_{\text{CR}}-1)\frac{c}{H_0 \lambda_{\text{BH}}}} \frac{2}{3\Omega_M} \left\{ \sqrt{\Omega_M(1+z_{\text{max}})^3 + \Omega_\Lambda} - \sqrt{\Omega_M(1+z_{\text{BH}})^3 + \Omega_\Lambda} \right\} \right]. \end{aligned} \quad (\text{B8})$$

In this case, we focus on the leading terms of  $O(c/H_0 \lambda_{\text{BH}})$  after integrating the formula over  $z_s$ .

The UHECR intensity at an energy below  $E_{\text{BH}}$  is obtained based on the sum of Eqs. B5 and B8.

### 3. $E_{\text{BH}} < E_i, \varepsilon_i \leq E_{\text{GZK}}/(1+z_s)$ - The region of BH process and redshift loss

In the energy region above  $E_{\text{BH}}$  but for sources with an emitted UHECR energy that is less than the photopion production threshold energy  $\varepsilon_{\text{GZK}} = E_{\text{GZK}}/(1+z_s)$ , the UHECR energy loss profile during the propagation is governed by the BH process and the redshift loss during the entire path from  $z = z_s$  to  $z = 0$ . Given that  $\varepsilon_i$  is related to the UHECR energy on the Earth by

$$\varepsilon_i = E_i(1+z_s)e^{-\frac{c}{H_0\lambda_{\text{BH}}}\frac{2}{3\Omega_{\text{M}}}\{\sqrt{\Omega_{\text{M}}(1+z_s)^3+\Omega_{\Lambda}}-1\}}, \quad (\text{B9})$$

the condition of  $\varepsilon_i \leq E_{\text{GZK}}/(1+z_s)$  can be rewritten as the boundary condition of  $z_s$ :

$$\sqrt{\Omega_{\text{M}}(1+z_s)^3+\Omega_{\Lambda}} \leq 1 + \frac{H_0\lambda_{\text{BH}}}{c}\frac{3\Omega_{\text{M}}}{2}\ln\left(\frac{E_{\text{GZK}}}{E_i(1+z_s)^2}\right). \quad (\text{B10})$$

It sets the maximal redshift of the sources that constitute the left and right-hand-side in the preceding equation to be equal to each other. Denoting this solution by  $\overline{z_{\text{BH}}^{\text{GZK}}}(E_i)$ , the upper bound in the redshift integral of Eq. B3,  $z_{\text{UB}}$ , is described by  $z_{\text{BH}}^{\text{GZK}}(E_i)$ , which is a function of  $E_i$  and classified in a similar form to Eq. B4 as

$$1 + z_{\text{BH}}^{\text{GZK}} = \begin{cases} 1 + z_{\text{max}} & \left(E_i < \overline{z_{\text{BH}}^{\text{GZK}}^{-1}}(z_{\text{max}})\right) \\ 1 + \overline{z_{\text{BH}}^{\text{GZK}}}(E_i) & \left(\overline{z_{\text{BH}}^{\text{GZK}}^{-1}}(z_{\text{max}}) \leq E_i < \overline{z_{\text{BH}}^{\text{GZK}}^{-1}}(0)\right) \\ 1 & \left(\overline{z_{\text{BH}}^{\text{GZK}}^{-1}}(0) \leq E_i\right), \end{cases} \quad (\text{B11})$$

since the source redshift  $z_s$  is in the range of  $z_s = 0$  and  $z_s = z_{\text{max}}$ . In this case  $\overline{z_{\text{BH}}^{\text{GZK}}^{-1}}$  is an inverse function that resolves  $z = \overline{z_{\text{BH}}^{\text{GZK}}}(E_i)$ .

The UHECR spectrum from a source is given by

$$\frac{d\dot{N}_{\text{CR}}}{dE_i} = \frac{K_{\text{CR}}}{\varepsilon_{i0}}(1+z_s)^{-(\alpha_{\text{CR}}-1)}\left(\frac{E_i}{\varepsilon_{i0}}\right)^{-\alpha_{\text{CR}}} e^{-(\alpha_{\text{CR}}-1)\frac{c}{H_0\lambda_{\text{BH}}}\frac{2}{3\Omega_{\text{M}}}\{\sqrt{\Omega_{\text{M}}(1+z_s)^3+\Omega_{\Lambda}}-1\}}. \quad (\text{B12})$$

The redshift integral represented by Eq. B3 with  $z_{\text{UB}} = z_{\text{BH}}^{\text{GZK}}$  and  $z_{\text{LB}} = 0$  then gives the UHECR source intensity from sources with  $z_s \leq z_{\text{BH}}^{\text{GZK}}$ . We obtain

$$\frac{dJ_{\text{CR}}}{dE_i} \simeq n_0 \frac{K_{\text{CR}}}{\varepsilon_{i0}} \lambda_{\text{BH}} \left(\frac{E_i}{\varepsilon_{i0}}\right)^{-\alpha_{\text{CR}}} \frac{1}{\alpha_{\text{CR}}-1} \left[ \left(1 + \frac{m-\alpha_{\text{CR}}-2}{\alpha_{\text{CR}}-1} \frac{H_0\lambda_{\text{BH}}}{c}\right) - \left\{ (1+z_{\text{BH}}^{\text{GZK}})^{m-\alpha_{\text{CR}}-2} + \frac{m-\alpha_{\text{CR}}-2}{\alpha_{\text{CR}}-1} \frac{H_0\lambda_{\text{BH}}}{c} (1+z_{\text{BH}}^{\text{GZK}})^{m-\alpha_{\text{CR}}-5} \right\} e^{-(\alpha_{\text{CR}}-1)\frac{c}{H_0\lambda_{\text{BH}}}\frac{2}{3\Omega_{\text{M}}}\{\sqrt{\Omega_{\text{M}}(1+z_{\text{BH}}^{\text{GZK}})^3+\Omega_{\Lambda}}-1\}} \right]. \quad (\text{B13})$$

In this case, we keep terms up to the second-order for  $O(c/H_0\lambda_{\text{BH}})$  when we integrate the formula over  $z_s$ .

### 4. $E_{\text{GZK}}/(1+z_s) < E_i, E_i < E_{\text{GZK}}$ - The region of partial GZK and BH process

In this energy range, the UHECR energy loss profile is similar to that described in section B2, but now involves photopion production. UHECRs emitted from a source at  $z = z_s$  lose their energies via photopion production until their energies become less than the threshold energy of the photo-hadronic interactions. The BH pair production and the redshift energy loss determines the UHECR energy profile thereafter. This transition occurs at a redshift of  $z = z_{\text{BH}}^{\text{GZK}}$ . The UHECR energy on the Earth  $E_i$  is then written as

$$E_i = \frac{E_{\text{GZK}}}{(1+z_{\text{BH}}^{\text{GZK}})^2} e^{-\frac{c}{H_0\lambda_{\text{BH}}}\frac{2}{3\Omega_{\text{M}}}\{\sqrt{\Omega_{\text{M}}(1+z_{\text{BH}}^{\text{GZK}})^3+\Omega_{\Lambda}}-1\}}. \quad (\text{B14})$$

It should be noted that  $z_{\text{BH}}^{\text{GZK}}$  is related to the UHECR energy at a source of  $\varepsilon_i$  since  $\varepsilon_i$  is associated with  $E_{\text{GZK}}$  via the photopion production and redshift energy loss during the propagation from  $z = z_s$  to  $z = z_{\text{BH}}^{\text{GZK}}$ . It is given by

$$\varepsilon_i = E_{\text{GZK}} \frac{(1+z_s)}{(1+z_{\text{BH}}^{\text{GZK}})^2} e^{-\frac{c}{H_0 \lambda_{\text{GZK}}} \frac{2}{3\Omega_M} \{\sqrt{\Omega_M(1+z_s)^3 + \Omega_\Lambda} - \sqrt{\Omega_M(1+z_{\text{BH}}^{\text{GZK}})^3 + \Omega_\Lambda}\}}. \quad (\text{B15})$$

The UHECR spectrum is calculated as

$$\begin{aligned} \frac{d\dot{N}_{\text{CR}}}{dE_i} &= \int d\varepsilon_i \frac{d\dot{N}_{\text{CR}}}{d\varepsilon_i} \delta\left(E_i - \frac{E_{\text{GZK}}}{(1+z_{\text{BH}}^{\text{GZK}})^2} e^{-\frac{c}{H_0 \lambda_{\text{BH}}} \frac{2}{3\Omega_M} \{\sqrt{\Omega_M(1+z_{\text{BH}}^{\text{GZK}})^3 + \Omega_\Lambda} - 1\}}\right) \\ &= \frac{c}{H_0 \lambda_{\text{GZK}}} \frac{K_{\text{CR}}}{\varepsilon_{i0}} (1+z_s)^{-(\alpha_{\text{CR}}-1)} \left(\frac{E_{\text{GZK}}}{\varepsilon_{i0}}\right)^{-\alpha_{\text{CR}}} (1+z_{\text{BH}}^{\text{GZK}})^{2\alpha_{\text{CR}}-2} \frac{1}{2\sqrt{\Omega_M(1+z_{\text{BH}}^{\text{GZK}})^3 + \Omega_\Lambda} + \frac{c}{H_0 \lambda_{\text{BH}}} \frac{1}{(1+z_{\text{BH}}^{\text{GZK}})^2}} \times \\ &\quad e^{-\frac{c}{H_0 \lambda_{\text{BH}}} \frac{2}{3\Omega_M} \{\sqrt{\Omega_M(1+z_{\text{BH}}^{\text{GZK}})^3 + \Omega_\Lambda} - 1\}} - (\alpha_{\text{CR}}-1) \frac{c}{H_0 \lambda_{\text{GZK}}} \frac{2}{3\Omega_M} \{\sqrt{\Omega_M(1+z_s)^3 + \Omega_\Lambda} - \sqrt{\Omega_M(1+z_{\text{BH}}^{\text{GZK}})^3 + \Omega_\Lambda}\}. \end{aligned} \quad (\text{B16})$$

Using Eq. B3 with  $z_{\text{UB}} = z_{\text{max}}$  and  $z_{\text{LB}} = z_{\text{BH}}^{\text{GZK}}$ , the UHECR intensity is then written as

$$\begin{aligned} \frac{dJ_{\text{CR}}}{dE_i} &= \frac{c}{H_0} n_0 \frac{K_{\text{CR}}}{\varepsilon_{i0}} \left(\frac{E_{\text{GZK}}}{\varepsilon_{i0}}\right)^{-\alpha_{\text{CR}}} \frac{1}{\alpha_{\text{CR}} - 1} (1+z_{\text{BH}}^{\text{GZK}})^{2\alpha_{\text{CR}}-2} \frac{e^{-\frac{c}{H_0 \lambda_{\text{BH}}} \frac{2}{3\Omega_M} \{\sqrt{\Omega_M(1+z_{\text{BH}}^{\text{GZK}})^3 + \Omega_\Lambda} - 1\}}}{2\sqrt{\Omega_M(1+z_{\text{BH}}^{\text{GZK}})^3 + \Omega_\Lambda} + \frac{c}{H_0 \lambda_{\text{BH}}} \frac{1}{(1+z_{\text{BH}}^{\text{GZK}})^2}} \times \\ &\quad \left[ (1+z_{\text{BH}}^{\text{GZK}})^{m-\alpha_{\text{CR}}-2} - (1+z_{\text{max}})^{m-\alpha_{\text{CR}}-2} e^{-(\alpha_{\text{CR}}-1) \frac{c}{H_0 \lambda_{\text{GZK}}} \frac{2}{3\Omega_M} \{\sqrt{\Omega_M(1+z_{\text{max}})^3 + \Omega_\Lambda} - \sqrt{\Omega_M(1+z_{\text{BH}}^{\text{GZK}})^3 + \Omega_\Lambda}\}} \right]. \end{aligned} \quad (\text{B17})$$

In this case, we only focus on the first-order terms of  $O(c/H_0 \lambda_{\text{GZK}})$ .

The UHECR intensity at an energy between  $E_{\text{BH}}$  and  $E_{\text{GZK}}$  is obtained by the sum of Eqs. B13 and B17.

### 5. $E_{\text{GZK}} \leq E_i$ - The region of GZK process only

UHECRs in this energy region only originate from a source within the GZK sphere of  $R \lesssim \lambda_{\text{GZK}}$ .  $\varepsilon_i$  is related to the UHECR energy on the Earth by

$$\varepsilon_i = E_i (1+z_s) e^{-\frac{c}{H_0 \lambda_{\text{GZK}}} \frac{2}{3\Omega_M} \{\sqrt{\Omega_M(1+z_s)^3 + \Omega_\Lambda} - 1\}}. \quad (\text{B18})$$

Repeating the similar described procedures, the UHECR intensity is given by

$$\frac{dJ_{\text{CR}}}{dE_i} \simeq n_0 \frac{K_{\text{CR}}}{\varepsilon_{i0}} \lambda_{\text{GZK}} \left(\frac{E_i}{\varepsilon_{i0}}\right)^{-\alpha_{\text{CR}}} \frac{1}{\alpha_{\text{CR}} - 1} \left[ 1 - (1+z_{\text{max}})^{m-\alpha_{\text{CR}}-2} e^{-(\alpha_{\text{CR}}-1) \frac{c}{H_0 \lambda_{\text{GZK}}} \frac{2}{3\Omega_M} \{\sqrt{\Omega_M(1+z_{\text{max}})^3 + \Omega_\Lambda} - 1\}} \right]. \quad (\text{B19})$$

Although we obtained the analytical formula of  $dJ_{\text{CR}}/dE_i$ , we numerically integrated the analytically obtained  $d\dot{N}_{\text{CR}}/dE_i$  over a source redshift in Eq. B3 to calculate UHECR flux in the presented study described in this report.

In the construction of the unification model, the energy density of UHECR protons are the most relevant, rather than the detailed spectral shape, because cosmic-ray proton emission power from sources at cosmological distances is directly related to the observed neutrino intensity. The applicability of the presented analytical formulation for estimating the energy density is demonstrated by comparisons between the estimate obtaining using the analytical formula and that obtained using a full numerical calculation. We refer to the setup of the ‘‘proton dip’’ model in Ref. [54] because it facilitates straightforward comparisons. The energy density per unit volume obtained based on robust numerical calculations for source evolution correspond to a star formation rate of  $7.5 \times 10^{44} \text{ erg yr}^{-1} \text{ Mpc}^{-3}$  ( $\alpha_{\text{CR}} = 2.5$ ) above  $10^{18} \text{ eV}$ , whereas we obtained  $9.3 \times 10^{44} \text{ erg yr}^{-1} \text{ Mpc}^{-3}$ . For a stronger evolution that represents powerful radio galaxies (FR-II), the full simulation gives  $4.2 \times 10^{44} \text{ erg yr}^{-1} \text{ Mpc}^{-3}$  ( $\alpha_{\text{CR}} = 2.3$ ) whereas the analytical formula yields  $3.4 \times 10^{44} \text{ erg yr}^{-1} \text{ Mpc}^{-3}$ . We determined that the present approximated analytical formula functions for the required precision of the generic unification model, considering that the other uncertainties of the source are larger than the accuracy we obtained.

- 
- [1] M. Aartsen *et al.* (IceCube Collaboration), Phys.Rev.Lett. **111**, 021103 (2013), arXiv:1304.5356 [astro-ph.HE].
- [2] M. Aartsen *et al.* (IceCube Collaboration), Science **342**, 1242856 (2013), arXiv:1311.5238 [astro-ph.HE].
- [3] M. Aartsen *et al.* (IceCube Collaboration), Phys.Rev.Lett. **113**, 101101 (2014), arXiv:1405.5303; <https://icecube.wisc.edu/science/data/HE-nu-2010-2014> [astro-ph.HE].
- [4] M. G. Aartsen *et al.* (IceCube Collaboration), Astrophys. J. **833**, 3 (2016), arXiv:1607.08006 [astro-ph.HE].
- [5] K. Murase, M. Ahlers, and B. C. Lacki, Phys.Rev. **D88**, 121301(R) (2013), arXiv:1306.3417 [astro-ph.HE].
- [6] K. Fang and K. Murase, Nature Phys. Lett. **14**, 396 (2018), arXiv:1704.00015 [astro-ph.HE].
- [7] B. Katz, E. Waxman, T. Thompson, and A. Loeb, (2013), arXiv:1311.0287 [astro-ph.HE].
- [8] K. Murase and E. Waxman, Phys. Rev. **D94**, 103006 (2016), arXiv:1607.01601 [astro-ph.HE].
- [9] M. Kachelriess, O. Kalashev, S. Ostapchenko, and D. Semikoz, Phys. Rev. D **96**, 083006 (2017), arXiv:1704.06893 [astro-ph.HE].
- [10] W. Winter, Phys.Rev. **D88**, 083007 (2013), arXiv:1307.2793 [astro-ph.HE].
- [11] E. Waxman and J. N. Bahcall, Phys.Rev.Lett. **78**, 2292 (1997), arXiv:astro-ph/9701231 [astro-ph].
- [12] E. Waxman and J. N. Bahcall, Astrophys.J. **541**, 707 (2000), arXiv:hep-ph/9909286 [hep-ph].
- [13] K. Murase, K. Ioka, S. Nagataki, and T. Nakamura, Astrophys.J. **651**, L5 (2006), arXiv:astro-ph/0607104 [astro-ph].
- [14] N. Gupta and B. Zhang, Astropart.Phys. **27**, 386 (2007), arXiv:astro-ph/0606744 [astro-ph].
- [15] B. T. Zhang and K. Murase, Phys. Rev. D **100**, 103004 (2019), arXiv:1812.10289 [astro-ph.HE].
- [16] K. Murase, P. Mészáros, and B. Zhang, Phys.Rev. **D79**, 103001 (2009), arXiv:0904.2509 [astro-ph.HE].
- [17] K. Fang, K. Kotera, K. Murase, and A. V. Olinto, Phys.Rev. **D90**, 103005 (2014), arXiv:1311.2044 [astro-ph.HE].
- [18] K. Fang, B. D. Metzger, K. Murase, I. Bartos, and K. Kotera, (2018), arXiv:1812.11673 [astro-ph.HE].
- [19] B. T. Zhang, K. Murase, F. Oikonomou, and Z. Li, Phys. Rev. D **96**, 063007 (2017), [Addendum: Phys.Rev.D 96, 069902 (2017)], arXiv:1706.00391 [astro-ph.HE].
- [20] C. Guépin, K. Kotera, E. Barausse, K. Fang, and K. Murase, Astron. Astrophys. **616**, A179 (2018), arXiv:1711.11274 [astro-ph.HE].
- [21] D. Biehl, D. Boncioli, C. Lunardini, and W. Winter, Sci. Rep. **8**, 10828 (2018), arXiv:1711.03555 [astro-ph.HE].
- [22] K. Mannheim, Astropart.Phys. **3**, 295 (1995).
- [23] A. Atoyan and C. D. Dermer, Phys.Rev.Lett. **87**, 221102 (2001), arXiv:astro-ph/0108053 [astro-ph].
- [24] W. Essey, O. E. Kalashev, A. Kusenko, and J. F. Beacom, Phys. Rev. Lett. **104**, 141102 (2010), arXiv:0912.3976 [astro-ph.HE].
- [25] K. Murase, C. D. Dermer, H. Takami, and G. Migliori, Astrophys. J. **749**, 63 (2012), arXiv:1107.5576 [astro-ph.HE].
- [26] K. Murase, Y. Inoue, and C. D. Dermer, Phys.Rev. **D90**, 023007 (2014), arXiv:1403.4089 [astro-ph.HE].
- [27] R. Blandford, Phys. Scripta T **85**, 191 (2000), arXiv:astro-ph/9906026.
- [28] M. Lemoine and E. Waxman, JCAP **11**, 009 (2009), arXiv:0907.1354 [astro-ph.HE].
- [29] A. Aab *et al.* (Pierre Auger), JCAP **04**, 038 (2017), [Erratum: JCAP 03, E02 (2018)], arXiv:1612.07155 [astro-ph.HE].
- [30] K. Murase, F. Oikonomou, and M. Petropoulou, Astrophys. J. **865**, 124 (2018), arXiv:1807.04748 [astro-ph.HE].
- [31] B. T. Zhang, K. Murase, S. S. Kimura, S. Horiuchi, and P. Mszros, Phys. Rev. D **97**, 083010 (2018), arXiv:1712.09984 [astro-ph.HE].
- [32] This difference is known to be important for model-dependent constraints on neutrinos from GRBs.
- [33] S. Yoshida and H. Takami, Phys.Rev. **D90**, 123012 (2014), arXiv:1409.2950 [astro-ph.HE].
- [34] C. D. Dermer, K. Murase, and H. Takami, Astrophys. J. **755**, 147 (2012), arXiv:1203.6544 [astro-ph.HE].
- [35] K. Murase, D. Guetta, and M. Ahlers, Phys. Rev. Lett. **116**, 071101 (2016), arXiv:1509.00805 [astro-ph.HE].
- [36] K. Murase and S. Nagataki, Phys. Rev. **D73**, 063002 (2006), arXiv:astro-ph/0512275 [astro-ph].
- [37] K. Murase, K. Ioka, S. Nagataki, and T. Nakamura, Phys.Rev. **D78**, 023005 (2008), arXiv:0801.2861 [astro-ph].
- [38] K. Murase and M. Fukugita, Phys. Rev. **D99**, 063012 (2019), arXiv:1806.04194 [astro-ph.HE].
- [39] K. Murase, Phys.Rev. **D76**, 123001 (2007), arXiv:0707.1140 [astro-ph].
- [40] H.-N. He, R.-Y. Liu, X.-Y. Wang, S. Nagataki, K. Murase, *et al.*, Astrophys.J. **752**, 29 (2012), arXiv:1204.0857 [astro-ph.HE].
- [41] S. S. Kimura, K. Murase, P. Mészáros, and K. Kiuchi, Astrophys. J. **848**, L4 (2017), arXiv:1708.07075 [astro-ph.HE].
- [42] T. Gaisser, *Cosmic rays and particle physics* (Cambridge University Press, Cambridge, England 1990).
- [43] S. Razzaque, P. Mészáros, and E. Waxman, Phys. Rev. Lett. **93**, 181101 (2004), [Erratum: Phys. Rev. Lett. 94, 109903 (2005)], arXiv:astro-ph/0407064 [astro-ph].
- [44] K. Murase, K. Asano, T. Terasawa, and P. Meszaros, Astrophys. J. **746**, 164 (2012), arXiv:1107.5575 [astro-ph.HE].
- [45] M. Aartsen *et al.* (IceCube), Phys. Rev. D **98**, 062003 (2018), arXiv:1807.01820 [astro-ph.HE].
- [46] M. G. Aartsen *et al.* (IceCube Collaboration), Phys. Rev. Lett. **117**, 241101 (2016), [Erratum: Phys. Rev. Lett.119,no.25,259902(2017)], arXiv:1607.05886 [astro-ph.HE].
- [47] K. Kotera, D. Allard, and A. Olinto, JCAP **10**, 013 (2010), arXiv:1009.1382 [astro-ph.HE].
- [48] S. Yoshida and A. Ishihara, Phys. Rev. D **85**, 063002 (2012), arXiv:1202.3522 [astro-ph.HE].
- [49] M. G. Aartsen *et al.* (IceCube Collaboration), in *Proceedings, 34th International Cosmic Ray Conference (ICRC 2015)* (2015) arXiv:1510.05223 [astro-ph.HE].
- [50] M. Aartsen *et al.* (IceCube), Phys. Rev. D **88**, 042004 (2013), arXiv:1307.3795 [astro-ph.HE].

- [51] F. Fenu (Pierre Auger), PoS **ICRC2017**, 486 (2018).
- [52] T. Abu-Zayyad *et al.* (Telescope Array), *Astrophys. J.* **768**, L1 (2013), arXiv:1205.5067 [astro-ph.HE].
- [53] E. Waxman and J. N. Bahcall, *Phys.Rev.* **D59**, 023002 (1998), arXiv:hep-ph/9807282 [hep-ph].
- [54] G. Decerprit and D. Allard, *Astron. Astrophys.* **535**, A66 (2011), arXiv:1107.3722 [astro-ph.HE].
- [55] S. Horiuchi, J. F. Beacom, C. S. Kochanek, J. L. Prieto, K. Z. Stanek, and T. A. Thompson, *Astrophys. J.* **738**, 154 (2011), arXiv:1102.1977 [astro-ph.CO].
- [56] A. Pe'er, K. Murase, and P. Mészáros, *Phys.Rev.* **D80**, 123018 (2009), arXiv:0911.1776 [astro-ph.HE].
- [57] K. Murase and J. F. Beacom, *Phys.Rev.* **D81**, 123001 (2010), arXiv:1003.4959 [astro-ph.HE].
- [58] M. Milgrom and V. Ussov, *Astrophys. J. Lett.* **449**, L37 (1995), arXiv:astro-ph/9505009.
- [59] E. Waxman, *Phys.Rev.Lett.* **75**, 386 (1995), arXiv:astro-ph/9505082 [astro-ph].
- [60] M. Vietri, *Astrophys. J.* **453**, 883 (1995), arXiv:astro-ph/9506081 [astro-ph].
- [61] N. Globus, D. Allard, R. Mochkovitch, and E. Parizot, *Mon. Not. Roy. Astron. Soc.* **451**, 751 (2015), arXiv:1409.1271 [astro-ph.HE].
- [62] D. Biehl, D. Boncioli, A. Fedynitch, and W. Winter, *Astron. Astrophys.* **611**, A101 (2018), arXiv:1705.08909 [astro-ph.HE].
- [63] P. Meszaros, *Rept. Prog. Phys.* **69**, 2259 (2006), arXiv:astro-ph/0605208.
- [64] F. Samuelsson, D. Bégué, F. Ryde, and A. Pe'er, *Astrophys. J.* **876**, 93 (2019), arXiv:1810.06579 [astro-ph.HE].
- [65] D. Wanderman and T. Piran, *Mon. Not. Roy. Astron. Soc.* **448**, 3026 (2015), arXiv:1405.5878 [astro-ph.HE].
- [66] R. Abbasi *et al.* (IceCube Collaboration), *Nature* **484**, 351 (2012), arXiv:1204.4219 [astro-ph.HE].
- [67] M. Aartsen *et al.* (IceCube Collaboration), *Astrophys. J.* **805**, L5 (2015), arXiv:1412.6510 [astro-ph.HE].
- [68] M. Aartsen *et al.* (IceCube Collaboration), *Astrophys. J.* **843**, 112 (2017), arXiv:1702.06868 [astro-ph.HE].
- [69] M. Bustamante, P. Baerwald, K. Murase, and W. Winter, *Nature Communications* **6**, 6783 (2015), arXiv:1409.2874 [astro-ph.HE].
- [70] M. Bustamante, K. Murase, W. Winter, and J. Heinze, *Astrophys. J.* **837**, 33 (2017), arXiv:1606.02325 [astro-ph.HE].
- [71] X.-Y. Wang, S. Razzaque, P. Mészáros, and Z.-G. Dai, *Phys.Rev.* **D76**, 083009 (2007), arXiv:0705.0027 [astro-ph].
- [72] A. M. Soderberg *et al.*, *Nature* **442**, 1014 (2006), arXiv:astro-ph/0604389.
- [73] R. Margutti *et al.*, *Astrophys. J.* **872**, 18 (2019), arXiv:1810.10720 [astro-ph.HE].
- [74] D. Coppejans *et al.*, *Astrophys. J.* **895**, L23 (2020), arXiv:2003.10503 [astro-ph.HE].
- [75] F. Samuelsson, D. Bégué, F. Ryde, A. Pe'er, and K. Murase, (2020), arXiv:2005.02417 [astro-ph.HE].
- [76] S. Campana *et al.*, *Nature* **442**, 1008 (2006), arXiv:astro-ph/0603279 [astro-ph].
- [77] E. Liang, B. Zhang, and Z. Dai, *Astrophys. J.* **662**, 1111 (2007), arXiv:astro-ph/0605200 [astro-ph].
- [78] D. Biehl, J. Heinze, and W. Winter, *Mon. Not. Roy. Astron. Soc.* **476**, 1191 (2018), arXiv:1712.00449 [astro-ph.HE].
- [79] K. Kashiyama, K. Murase, and P. Mészáros, *Phys. Rev. Lett.* **111**, 131103 (2013), arXiv:1304.1945 [astro-ph.HE].
- [80] N. Senno, K. Murase, and P. Mészáros, *Phys. Rev.* **D93**, 083003 (2016), arXiv:1512.08513 [astro-ph.HE].
- [81] T. A. Thompson, P. Chang, and E. Quataert, *Astrophys. J.* **611**, 380 (2004), arXiv:astro-ph/0401555.
- [82] J. Dexter and D. Kasen, *Astrophys. J.* **772**, 30 (2013), arXiv:1210.7240 [astro-ph.HE].
- [83] N. Smith and R. McCray, *Astrophys. J. Lett.* **671**, L17 (2007), arXiv:0710.3428 [astro-ph].
- [84] J. Arons, *Astrophys. J.* **589**, 871 (2003), arXiv:astro-ph/0208444.
- [85] D. Burrows *et al.*, *Nature* **476**, 421 (2011), arXiv:1104.4787 [astro-ph.HE].
- [86] G. R. Farrar and A. Gruzinov, *Astrophys. J.* **693**, 329 (2009), arXiv:0802.1074 [astro-ph].
- [87] N. Senno, K. Murase, and P. Meszaros, *Astrophys. J.* **838**, 3 (2017), arXiv:1612.00918 [astro-ph.HE].
- [88] G. R. Farrar and T. Piran, (2014), arXiv:1411.0704 [astro-ph.HE].
- [89] R. Stein (IceCube), PoS **ICRC2019**, 1016 (2020), arXiv:1908.08547 [astro-ph.HE].
- [90] R. Stein *et al.*, (2020), arXiv:2005.05340 [astro-ph.HE].
- [91] W. Winter and C. Lunardini, (2020), arXiv:2005.06097 [astro-ph.HE].
- [92] K. Murase, S. S. Kimura, B. T. Zhang, F. Oikonomou, and M. Petropoulou, (2020), arXiv:2005.08937 [astro-ph.HE].
- [93] H. Takami and K. Sato, *Astropart. Phys.* **30**, 306 (2009), arXiv:0807.3442 [astro-ph].
- [94] K. Fang and K. Kotera, *Astrophys. J. Lett.* **832**, L17 (2016), arXiv:1610.08055 [astro-ph.HE].
- [95] K. Murase and H. Takami, *Astrophys. J.* **690**, L14 (2009), arXiv:0810.1813 [astro-ph].
- [96] B. Nizamov and M. Pshirkov, *JCAP* **03**, 060 (2020), arXiv:1804.01064 [astro-ph.HE].
- [97] M. G. Aartsen *et al.* (IceCube, Fermi-LAT, MAGIC, AGILE, ASAS-SN, HAWC, H.E.S.S., INTEGRAL, Kanata, Kiso, Kapteyn, Liverpool Telescope, Subaru, Swift NuSTAR, VERITAS, and VLA/17B-403 Collaborations), *Science* **361**, eaat1378 (2018), arXiv:1807.08816 [astro-ph.HE].
- [98] A. Keivani *et al.* (AMON Collaboration), *Astrophys. J.* **864**, 84 (2018), arXiv:1807.04537 [astro-ph.HE].
- [99] G. Ghisellini, F. Tavecchio, L. Foschini, G. Ghirlanda, L. Maraschi, and A. Celotti, *Mon. Not. Roy. Astron. Soc.* **402**, 497 (2010), arXiv:0909.0932 [astro-ph.CO].
- [100] M. Petropoulou, S. Coenders, and S. Dimitrakoudis, *Astropart. Phys.* **80**, 115 (2016), arXiv:1603.06954 [astro-ph.HE].
- [101] I. Liodakis and M. Petropoulou, *Astrophys. J. Lett.* **893**, L20 (2020), arXiv:2003.10460 [astro-ph.HE].
- [102] X. Rodrigues, A. Fedynitch, S. Gao, D. Boncioli, and W. Winter, *Astrophys. J.* **854**, 54 (2018), arXiv:1711.02091 [astro-ph.HE].
- [103] F. Tavecchio, G. Ghisellini, and D. Guetta, *Astrophys. J.* **793**, L18 (2014).
- [104] M. Petropoulou, S. Dimitrakoudis, P. Padovani, A. Mastichiadis, and E. Resconi, *Mon. Not. Roy. Astron. Soc.* **448**, 2412 (2015), arXiv:1501.07115 [astro-ph.HE].
- [105] P. Padovani, M. Petropoulou, P. Giommi, and E. Resconi, *Mon. Not. Roy. Astron. Soc.* **452**, 1877 (2015), arXiv:1506.09135 [astro-ph.HE].
- [106] C. D. Dermer, K. Murase, and Y. Inoue, *JHEAp* **3-4**,

- 29 (2014), arXiv:1406.2633 [astro-ph.HE].
- [107] However, cosmic-ray reservoir models use the spectral index of cosmic rays that are injected into the environment after they escape from the sources [6].
- [108] H. Takami, K. Murase, S. Nagataki, and K. Sato, *Astropart.Phys.* **31**, 201 (2009), arXiv:0704.0979 [astro-ph].